LAMPIRAN

LAMPIRAN 1

- Perhitungan mencari densitas pada papan partikel PJA
- Spesimen Papan Pertikel Lapisan 3

$$\rho = \frac{m}{v}$$

$$V = p\ x\ l\ x\ t$$

$$V = 0.0094 \times 0.1000 \times 0{,}0094$$

$$V = 8.04 \times 10^{-13} m^3$$

$$\rho = \frac{7.0\ x\ 10^{-5}\ kg}{1.33\ x\ 10^{-9}\ m^3} = 752.68\ kg/m^3$$

- Spesimen Papan Partikel Lapisan 6

$$\rho = \frac{m}{v}$$

$$V = p\ x\ l\ x\ t$$

$$V = 0.0994 \times 0.1000 \times 0{,}0109$$

$$V = 1.0 \times 10^{-12} m^3$$

$$\rho = \frac{7.2\ x\ 10^{-5}\ kg}{1.0\ x\ 10^{-12}\ m^3} = 666.6\ kg/m^3$$

- Perhitungan mencari densitas pada papan partikel PJB
- Spesimen Papan Pertikel Lapisan 3

$$\rho = \frac{m}{v}$$

$$V = p\ x\ l\ x\ t$$

$$V = 0.1006 \times 0.1008 \times 0{,}1125$$

$$V = 1.33 \times 10^{-9} m^3$$

$$\rho = \frac{7.2x\ 10^{-5}\ kg}{1.33\ x\ 10^{-9}\ m^3} = 50.71\ kg/m^3$$

- Spesimen Papan Partikel Lapisan 6

$$\rho = \frac{m}{v}$$

$$V = p\ x\ l\ x\ t$$

$$V = 0.1006 \times 0.1008 \times 0{,}1137$$

$$V = 1.33 \times 10^{-9} m^3$$

$$\rho = \frac{7.7\ x\ 10^{-5}\ kg}{1.33\ x\ 10^{-9}\ m^3} = 66.95\ kg/m^3$$

LAMPIRAN 2

Dokumentasi

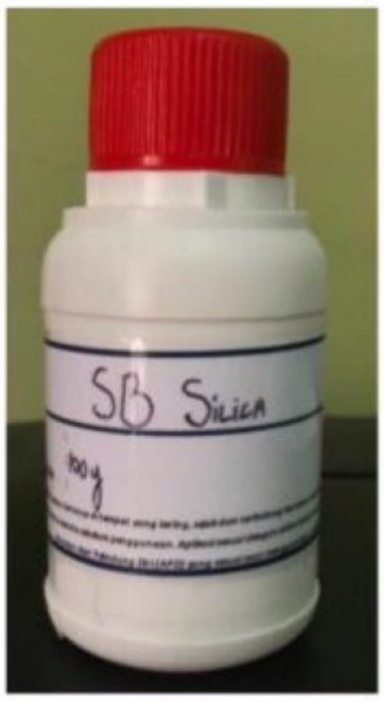

Cairan Silica Dispersi nanopartikel solvent-based

Proses Spraying

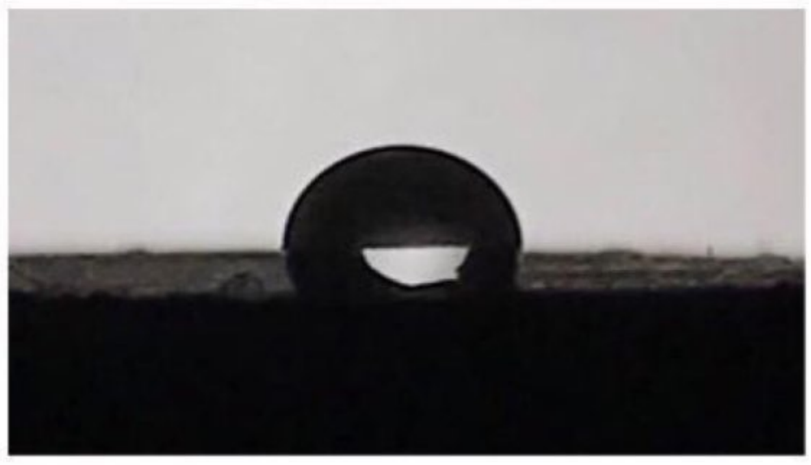

Pengujian Contact Angle

JAPAN

EDICT OF GOVERNMENT

In order to promote public education and public safety, equal justice for all, a better informed citizenry, the rule of law, world trade and world peace, this legal document is hereby made available on a noncommercial basis, as it is the right of all humans to know and speak the laws that govern them.

JIS A 5908 (2003) (English): Particleboards

安倍

The citizens of a nation must honor the laws of the land.

Fukuzawa Yukichi

BLANK PAGE

BLANK PAGE

JIS

JAPANESE
INDUSTRIAL
STANDARD

Translated and Published by
Japanese Standards Association

JIS A 5908 : 2003

Particleboards

ICS 79.060.20

Reference number : JIS A 5908 : 2003 (E)

Foreword

This translation has been made based on the original Japanese Industrial Standard revised by the Minister of Economy, Trade and Industry through deliberations at the Japanese Industrial Standards Committee in accordance with the Industrial Standardization Law. Consequently **JIS A 5908** : 1994 is replaced with **JIS A 5908** : 2003.

Attention is drawn to the possibility that some parts of this Standard may conflict with a patent right, application for a patent after opening to the public, utility model right or application for registration of utility model after opening to the public which have technical properties. The relevant Minister and the Japanese Industrial Standards Committee are not responsible for identifying the patent right, application for a patent after opening to the public, utility model right or application for registration of utility model after opening to the public which have the said technical properties.

Date of Establishment: 1957-09-16

Date of Revision: 2003-03-20

Date of Public Notice in Official Gazette: 2003-03-20

Investigated by: Japanese Industrial Standards Committee

Standards Board

Technical Committee on Architecture

JIS A 5908 : 2003, First English edition published in 2003-05

Translated and published by: Japanese Standards Association
4-1-24, Akasaka, Minato-ku, Tokyo, 107-8440 JAPAN

In the event of any doubts arising as to the contents,
the original JIS is to be the final authority.

Contents

Particleboards

1 Scope This Japanese Industrial Standard specifies the boards which are formed mainly from wood particles(1) by hot pressing with adhesives (hereafter referred to as "particleboard").

Note (1) The wood particles include chip, flake, wafer, strand, etc.

2 Normative references The standards shown in Attached Table 1 contain provisions which, through reference in this Standard, constitute provisions of this Standard. The most recent editions of the standards (including amendments) shall be applied.

3 Classification and symbols The particleboard shall be classified as given below according to the condition of the face and back, bending strength, adhesives, emission quantity of formaldehyde, and incombustibility.

a) **Classification according to condition of face and back** Classification according to the condition of face and back shall be as specified in Table 1.

Table 1 Classification according to condition of face and back

Classification		Symbol	Condition of face and back
Base particleboard	Non-polished board	RN	Both sides are of base material, and non-polished.
	Polished board	RS	Both sides are of base material, and polished.
Veneered particleboard	Non-polished board	VN	Veneered on both sides of base particleboard, and non-polished.
	Polished board	VS	Veneered on both sides of base particleboard, and polished.
Decorative particleboard	Veneer overlay	DV	Decorative veneer is adhered to both sides or either side of base particleboard.
	Plastic overlay	DO	Sheet or film of synthetic resin type, impregnated paper of synthetic resin type, coat paper, after-coat paper or the like is adhered to both sides or either side of base particleboard, including non-patterned products where the decorative surface is finished in single colour and products with graining or abstract patterns.
	Coated	DC	Coating of synthetic resin type is heated and hardened, or printed on both sides or either side of base particleboard, including non-patterned products where the decorative surface is finished in single colour and products with graining or abstract patterns.

b) **Classification according to bending strength** Classification according to the bending strength shall be as specified in Table 2.

Table 2 Classification according to bending strength

Classification		Symbol	Bending strength
Base particleboard and decorative particleboard	Type 18	18	The bending strength shall be 18.0 N/mm² or over both lengthwise and widthwise.
	Type 13	13	The bending strength shall be 13.0 N/mm² or over both lengthwise and widthwise.
	Type 8	8	The bending strength shall be 8.0 N/mm² or over both lengthwise and widthwise.
Base particleboard	Type 24-10	24-10	The bending strength shall be 24.0 N/mm² or over lengthwise and 10.0 N/mm² or over widthwise.
	Type 17.5-10.5	17.5-10.5	The bending strength shall be 17.5 N/mm² or over lengthwise and 10.5 N/mm² or over widthwise.
Veneered particleboard	Type 30-15	30-15	The bending strength shall be 30.0 N/mm² or over lengthwise and 15.0 N/mm² or over widthwise.

Remarks : Type 24-10 means the board of the orientation strand (OSB) type, and Type 17.5-10.5 means the board of wafer type.

c) **Classification according to adhesives** Classification according to the adhesives shall be as specified in Table 3.

Table 3 Classification according to adhesives

Classification	Symbol	Adhesive	Main use (informative)
Type U	U	Urea resin type or at least equivalent in performance.	Suitable for furniture and cabinets.
Type M	M	Urea-melamine resin condensation type or at least equivalent in performance.	Suitable for floor substrates, roof substrates, inner and outer wall substrates, fixture materials or the like.
Type P	P	Phenolic resin type or at least equivalent in performance.	

d) **Classification according to emission quantity of formaldehyde** Classification according to the emission quantity of formaldehyde shall be as specified in Table 4.

Table 4 Classification according to emission quantity of formaldehyde

Classification	Symbol	Emission quantity of formaldehyde	
		mean	maximum
F☆☆☆☆	F☆☆☆☆	0.3 mg/L or under	0.4 mg/L or under
F☆☆☆	F☆☆☆	0.5 mg/L or under	0.7 mg/L or under
F☆☆	F☆☆	1.5 mg/L or under	2.1 mg/L or under

e) **Classification according to incombustibility** Classification according to the incombustibility shall be as specified in Table 5.

Table 5 Classification according to incombustibility

Classification	Symbol
Incombustibility grade 2	Incombustibility 2
Incombustibility grade 3	Incombustibility 3
Regular	—

4 Shapes, dimensions and tolerances Shapes, dimensions and tolerances shall be as specified below. However, the dimensions of the made-to-order product shall be subjected to the agreement between the parties concerned with delivery, and the tolerances and the squareness shall be as specified in Table 7.

a) **Thickness** The thickness shall be as specified in Table 6.

Table 6 Thickness

Unit: mm

Thickness	9, 10, 12, 15, 18, 20, 25, 30, 35, 40

Remarks: The thickness of the base particleboards of Type 24-10 and Type 17.5-10.5 may be 9.5 mm, 11 mm, 12.7 mm, 16 mm, 19 mm and 28.5 mm.

b) **Width and length** The width and length shall be as specified in Fig. 1.

Unit: mm

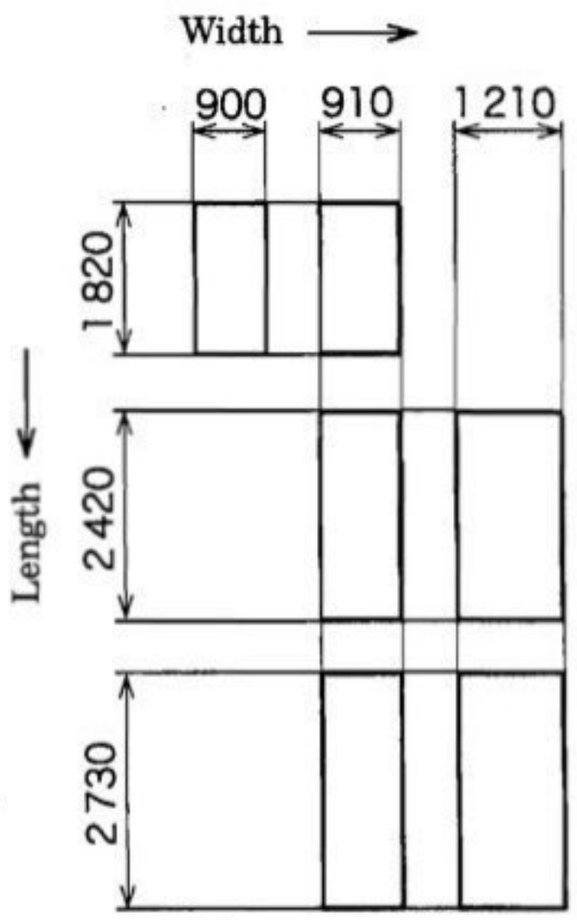

Fig. 1 Width and length

Remarks: The width and the length of the base particleboards of Type 24-10 and Type 17.5-10.5 may be 1 220 mm and 2 440 mm respectively.

c) **Tolerances and squareness** The tolerances and squareness shall be as specified in Table 7.

Table 7 Tolerances and squareness

Unit: mm

Classification	Thickness	Tolerances on thickness			Tolerances on width and length	Squareness
		Non-polished board	Polished board	Decorative board		
Base particleboard and veneered particleboard	Under 15	±1.0	±0.3	—	±3.0	2 max.
	15 or over to and excl. 20	±1.2				
	20 or over	±1.5				
Decorative particleboard	Under 18	—	—	±0.5		
	18 or over	—	—	±0.6		

Remarks : The thickness of the decorative particleboard means the thickness of the substrate added by the thickness of the decorative layer.

5 Appearance and quality

5.1 Appearance The appearance shall be as specified below:

a) The surfaces of the particleboards shall be free from noticeable unevenness, stains, exfoliations, etc., and any distortion or warpage detrimental to use, shall not be observed. The decorative particleboard shall be free from the defects as indicated in Table 8.

Table 8 Appearance of decorative particleboard

Classification of defects	Standard
Chippings (2), cracks or peelings	No defects shall be observed.
Distortion or warpage	No defects detrimental to use shall be observed.
Unevenness except for decorative purpose, dents, stains, flaws or mixing of foreign matters	Defects shall not be noticeably observed when visually checked at the position of 60 cm apart.
Irregular patterns, gloss and colour tone except for decorative purpose	Defects shall not be observed when visually checked at the position of 2 m (3) apart.

Notes (2) To mean the chipping of the substrates and decorative layers.

(3) To carry out the checking simultaneously with several test pieces arranged.

b) The section of the particleboard shall be excellent, and the side shall be square to the surface, except those whose sides are machined for the special purpose.

5.2 Quality The particleboard shall be tested on the quality items as indicated in Table 9 in accordance with test method in clause **6** and shall meet the requirements of Tables 10, 11, 12 and 13.

Table 9 Quality items

Quality item		Base particleboard and veneered particleboard			Decorative particleboard			Applicable subclause
		Type U	Type M	Type P	Type U	Type M	Type P	
Dimensions and squareness		○	○	○	○	○	○	**6.2**
Density		○	○	○	○	○	○	**6.3**
Water content		○	○	○	○	○	○	**6.4**
Bending strength		○	○	○	○	○	○	**6.5**
Bending strength under wet conditions (4)	Test A	—	○	—	—	○	—	**6.6**
	Test B	—	—	○	—	—	○	
Swelling in thickness after immersion in water (4)		—	○	○	—	○	○	**6.7**
Internal bond		○	○	○	○	○	○	**6.8**
Wood screw holding power (5)		○	○	○	○	○	○	**6.9**
Emission quantity of formaldehyde		○	○	○	○	○	○	**6.10**
In-plane tensile strength		—	—	—	○	○	○	**6.11**
Impact resistance		—	—	—	○	○	○	**6.12**
Acid resistance (6)		—	—	—	○	○	○	**6.13**
Alkali resistance (6)		—	—	—	○	○	○	**6.14**
Stain resistance (6)		—	—	—	○	○	○	**6.15**
Change-in-colour resistance (6)		—	—	—	○	○	○	**6.16**
Scratch resistance (6)		—	—	—	○	○	○	**6.17**
Thermal insulation		To be subjected to the agreement between the parties concerned with delivery.						**6.18**
Incombustibility (7)		○	○	○	○	○	○	**6.19**

Notes (4) Not to be applied to Type 8.

(5) The wood screw holding power shall be applied to the thickness of 15 mm or over.

(6) Not to be applied to the veneer overlay nor after-coat papers.

(7) To be applied to the particleboard having incombustibility.

Table 10 Quality

Classification			Density g/cm³	Moisture content %	Bending strength N/mm²		Bending strength under wet conditions (4) N/mm²		Swelling in thickness after immersion in water (4) %	Internal bond N/mm²	Wood screw holding power N	Emission quantity of formaldehyde mg/L	Bending Young's modulus (informative) N/mm²
					Lengthwise	Widthwise	Lengthwise	Widthwise					
Base particleboard, decorative particleboard	Type 18	F☆☆☆☆	0.40 or over up to and incl. 0.90	5 or over up to and incl. 13	18.0 min.		9.0 min.		12 max.	0.3 min.	500 min.	mean 0.3 or under maximum 0.4 or under	3 000 min. widthwise
		F☆☆☆										mean 0.5 or under maximum 0.7 or under	
		F☆☆										mean 1.5 or under maximum 2.1 or under	
	Type 13	F☆☆☆☆			13.0 min.		6.5 min.			0.2 min.	400 min.	mean 0.3 or under maximum 0.4 or under	2 500 min. widthwise
		F☆☆☆										mean 0.5 or under maximum 0.7 or under	
		F☆☆										mean 1.5 or under maximum 2.1 or under	
	Type 8	F☆☆☆☆			8.0 min.		—			0.15 min.	300 min.	mean 0.3 or under maximum 0.4 or under	2 000 min. widthwise
		F☆☆☆										mean 0.5 or under maximum 0.7 or under	
		F☆☆										mean 1.5 or under maximum 2.1 or under	

Table 10 (concluded)

Classification			Density g/cm³	Moisture content %	Bending strength N/mm²		Bending strength under wet conditions(4) N/mm²		Swelling in thickness after immersion in water(4) %	Internal bond N/mm²	Wood screw holding power N	Emission quantity of formaldehyde mg/L	Bending Young's modulus (informative) N/mm²
					Lengthwise	Widthwise	Lengthwise	Widthwise					
Base particleboard	Type 24-10	F☆☆☆☆	0.40 or over up to and incl. 0.90	5 or over up to and incl. 13	24.0 min.	10.0 min.	12.0 min.	5.0 min.	When the thickness is 12.7 mm or under, the required value shall be 25 or under. When the thickness is over 2.7 mm, the required value shall be 20 or under.	0.3 min.	500 min.	mean 0.3 or under maximum 0.4 or under	4 000 min. lengthwise, 1 300 min. widthwise
		F☆☆☆										mean 0.5 or under maximum 0.7 or under	
		F☆☆										mean 1.5 or under maximum 2.1 or under	
	Type 17.5-10.5	F☆☆☆☆			17.5 min.	10.5 min.	8.8 min.	5.3 min.				mean 0.3 or under maximum 0.4 or under	3 000 min. lengthwise, 2 000 min. widthwise
		F☆☆☆										mean 0.5 or under maximum 0.7 or under	
		F☆☆										mean 1.5 or under maximum 2.1 or under	
Veneered particleboard	Type 30-15	F☆☆☆☆			30.0 min.	15.0 min.	15.0 min.	7.5 min.	12 max.			mean 0.3 or under maximum 0.4 or under	4 000 min. lengthwise, 2 800 min. widthwise
		F☆☆☆										mean 0.5 or under maximum 0.7 or under	
		F☆☆										mean 1.5 or under maximum 2.1 or under	

Remarks : Lengthwise means the longitudinal direction, while widthwise means the direction orthogonal thereto. In the case of the veneered particleboard, lengthwise means the direction of the fibres of the veneer, and widthwise means the direction orthogonal thereto.

Table 11 Quality of decorative particleboard

Moisture content %	In-plane tensile strength N/mm²	Impact resistance	Acid resistance	Alkali resistance	Stain resistance	Change-in-colour resistance		Scratch resistance
					Stain resistance against the crayon (red)	Appearance	Colour difference	
5 or over up to and incl. 13	0.4 min.	To be free from the radial cracks, fracture and peeling of the decorative layer, and the diameter of recesses to be 20 mm or under.	No dis-coloration shall be observed.	No dis-coloration shall be observed.	To be of Gray scale 3 or over	To be free from defects such as crazing and swell on the surface.	To be of Gray scale 4 or over, or of colour difference 3.0 or under	No noticeable scratches shall be observed.

Remarks : The acid resistance, the alkali resistance, the stain resistance, the change-in-colour resistance and the scratch resistance are not applied to the veneer overlay nor after-coat.

Table 12 Thermal insulation

Thickness mm	Thermal resistance m²·K/W	Thickness mm	Thermal resistance m²·K/W
10	0.060 or over	25	0.155 or over
12	0.077 or over	30	0.181 or over
15	0.095 or over	35	0.215 or over
18	0.112 or over	40	0.241 or over
20	0.120 or over		

Remarks : The thermal resistance value which is not indicated in Table 12 shall be obtained by the proportional interpolation.

Table 13 Incombustibility

Classification	Incombustibility
Incombustibility grade 2	Incombustibility grade 2
Incombustibility grade 3	Incombustibility grade 3
Regular	—

6 Test methods

6.1 Test pieces

6.1.1 Sampling of test piece The test pieces of the dimensions and the number specified in Table 14 shall be sampled for every test item from the portion in the vicinity of the centre of the original board except the peripheral part of the sample.

In the case of the decorative board with grooves on the decorative surface, the test piece shall be sampled including the groove part.

6.1.2 Conditioning of test piece The test pieces shall be kept under air-dry condition(8) or those which reach the constant weight(9) at the temperature 20 ± 2 °C, and the humidity (65 ± 5) %. The test piece to be used for the formaldehyde emission test shall be in accordance with **7.3** of **JIS A 1460**.

Notes (8) The air-dry condition mentioned here means the condition of the test pieces which have been left in a well-ventilated room for seven days or more.

(9) The constant weight means the value where the mass is measured for every 24 h, and the rate of change reaches 0.1 % or under.

Table 14 Dimensions and number of test pieces

Test item	Dimensions of test piece mm	The number of test pieces to be sampled from one board
Density test	100 × 100	1
Moisture content test	100 × 100	1
Bending strength test	Width 50 × length [span (10) + 50]	Lengthwise 1, widthwise 1
Bending strength test under wet conditions	Width 50 × length [span (10) + 50]	Lengthwise 1, widthwise 1
Test of swelling in thickness after immersion in water	50 × 50	1
Internal bond test	50 × 50	1
Test of wood screw holding power	50 × 100	1
Formaldehyde emission test	50 × 150	Two sets of the number where the total surface area of the test piece including the butt ends is close to 1 800 cm^2 (the fraction of 5 and over shall be counted as a unit and the rest be disregarded) shall be used.
In-plane tensile strength test	50 × 50	1
Impact resistance test	300 × 300	1
Acid resistance test	100 × 100	1
Alkali resistance test	100 × 100	1
Stain resistance test	100 × 100	1
Change-in-colour resistance test	150 × 150	1 (11)
Scratch resistance test	50 × 50	1
Thermal insulation test	900 × 900	1
Incombustibility test	220 × 220	1

Notes (10) The span shall be 15 times the nominal thickness, and 150 mm or over at the same time.

(11) 3 test pieces shall be prepared for the pattern board.

6.2 Measurement of dimensions and squareness The measurement of the dimensions and squareness shall be as specified below:

6.2.1 Thickness The thickness shall be measured at four points of 20 mm or over inside the peripheral sides as indicated in Fig. 2 by means of a measuring device having the accuracy of $\frac{1}{20}$ mm or finer, and the mean value of four measured values shall be employed. The part where the measuring device contacts with the surface of the sample shall be a circle of 6 mm or over in diameter. The convex part shall be measured in the case where unevenness is provided for the purpose of decoration.

Unit : mm

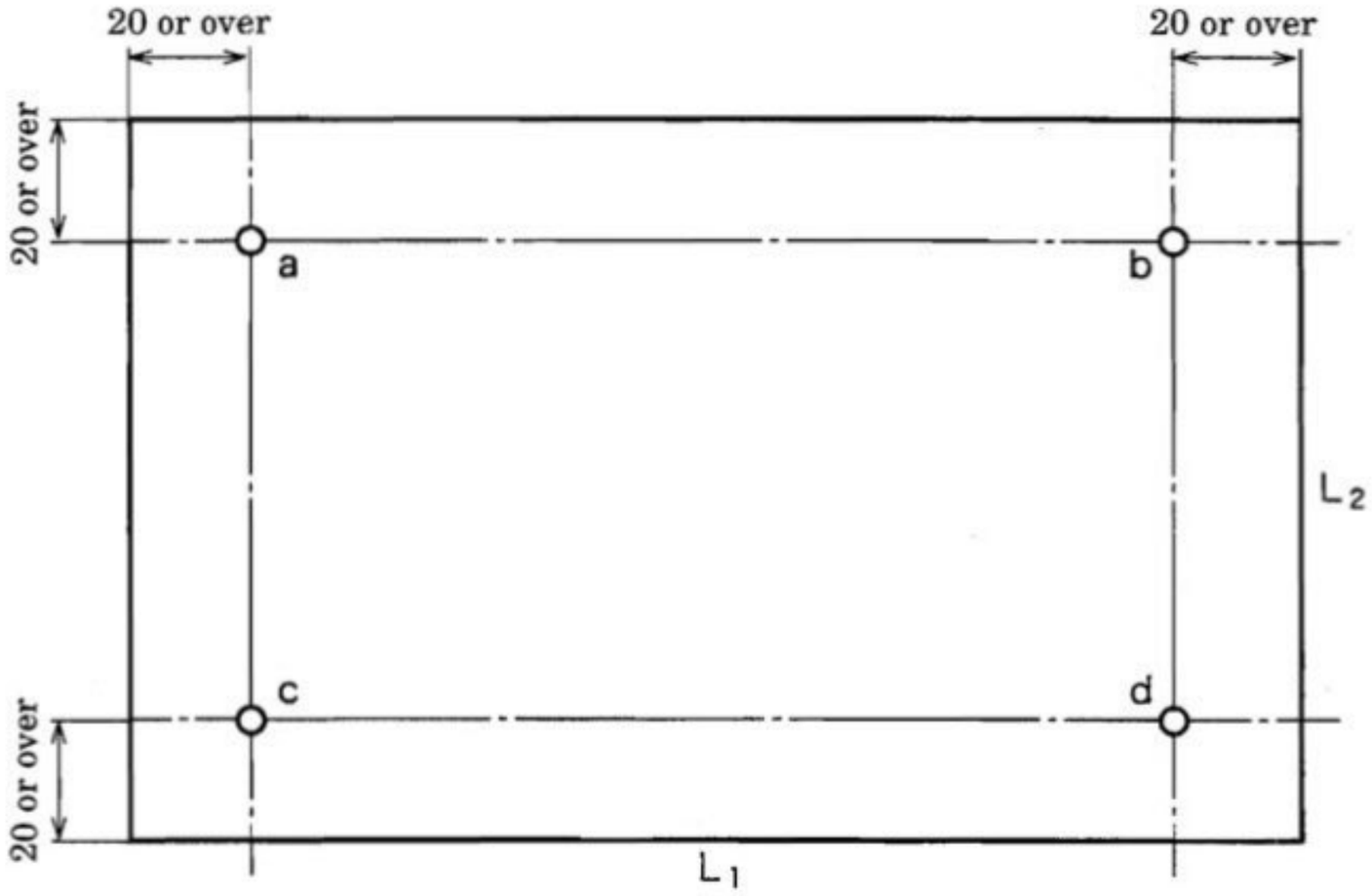

○: measuring point of thickness: four points at four corners (a, b, c, d) of 20 mm or over inside each side

Fig. 2 Measurement of thickness of product to be shipped

6.2.2 Width and length The width and length shall be measured by using a measuring device having the accuracy of 1 mm or finer. The measuring points of the width and length shall be about 100 mm inside the peripheral sides as indicated in Fig. 3, and the width and length are measured at two points parallel to each side respectively, and defined as the means value of the measured values.

Unit : mm

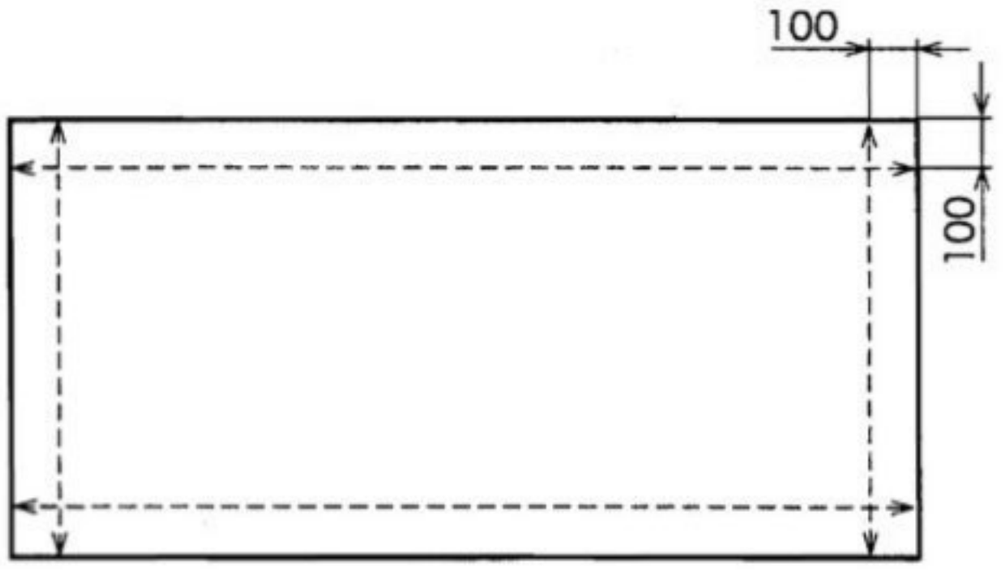

Fig. 3 Measurement of width and length of product

6.2.3 Squareness In defining the squareness, a sample shall be placed against the square of nominal size 1 000 of flat section square Grade 1 specified in **JIS B 7526** as indicated in Fig. 4, and the clearance (δ) to be generated between the square and the sample at the part of 1 000 mm apart from the corner shall be measured at four corners by means of a measuring device having the accuracy of 0.5 mm or finer.

When the side length (l) of the sample is under 1 000 mm, the clearance (δ) shall be measured at the end part of the side length, and the measured value shall be converted by the following formula:

$$\text{Converted clearance (mm)} = \frac{1\,000\delta}{l}$$

where, l : side length (mm) of the sample
δ : clearance (mm)

Unit : mm

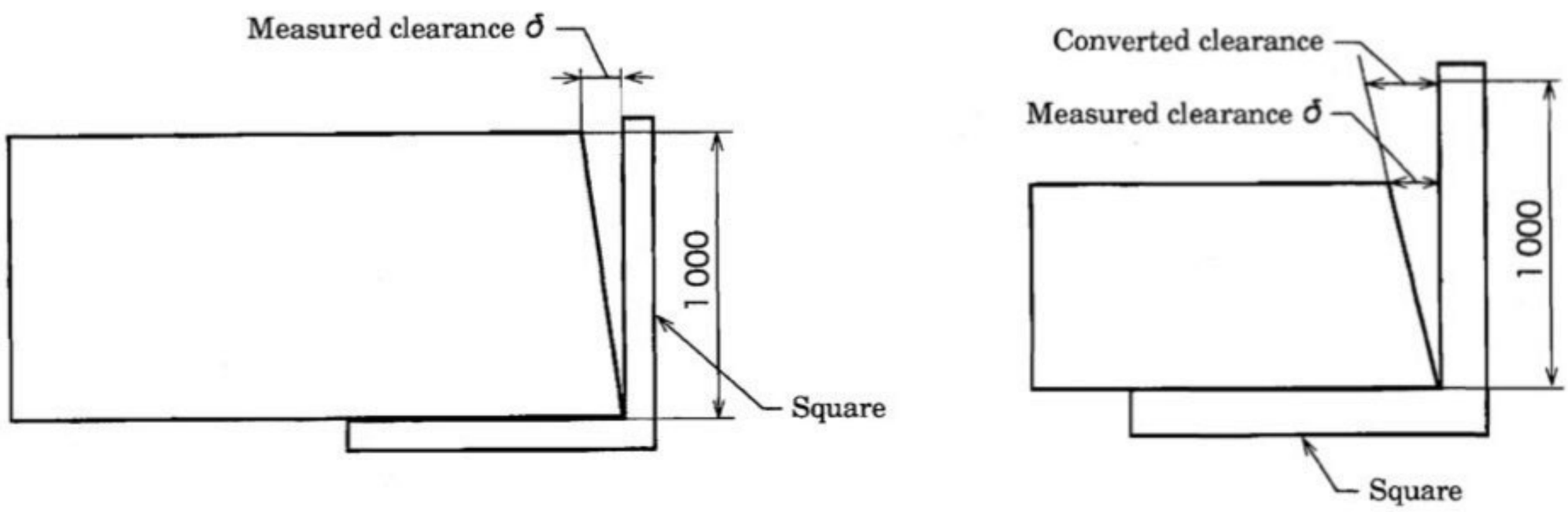

Fig. 4 Measurement of squareness

6.3 Density test Measure the lengths, widths and thicknesses of the points to be measured as shown in Fig. 5 and obtain their respective mean values to make them the length, width and thickness of the test piece with which the volume (V) is calculated. Then, measure the mass (m_1), and calculate the density by the formula below. In this case, the thickness, length, width and mass shall be measured to the nearest 0.05 mm, 0.1 mm, 0.1 mm and 0.1 g respectively, and the density shall be calculated to the nearest 0.01 g/cm^3.

$$\text{Density (g/cm}^3\text{)} = \frac{m_1}{V}$$

where, m_1 : mass (g)
V : volume (cm^3)

Unit : mm

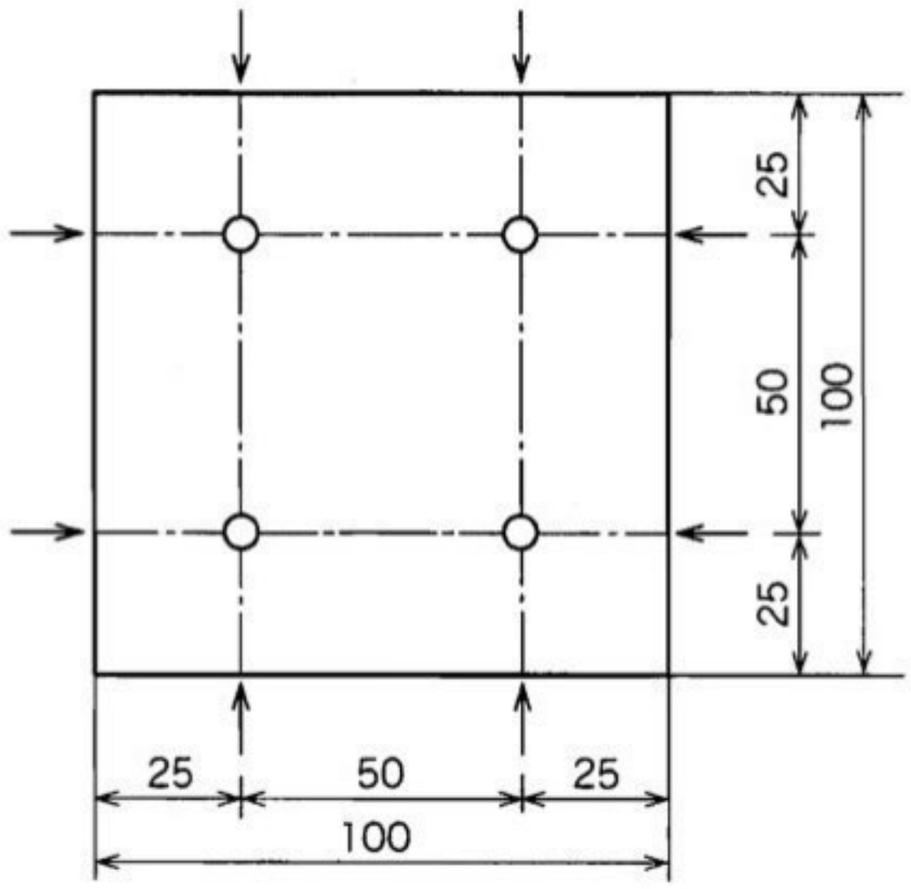

○: measuring points of thickness
↑: measuring points of width and length

Fig. 5 Points to be measured of length, width and thickness

6.4 Moisture content test Measure the mass (m_1) of a test piece, put it in an air drier kept at 103 ± 2 °C, measure the mass (m_0) when it has constant mass, and obtain the moisture content to the tenth's place by the following formula:

$$\text{Moisture content } (\%) = \frac{m_1 - m_0}{m_0} \times 100$$

where, m_0: mass (g) after drying
m_1: mass (g) before drying

6.5 Bending strength test Using the test apparatus shown in Fig. 6, apply a load of approximately 10 mm/min at a mean deformation speed from the surface of the test piece, and measure the maximum load (P). Calculate the bending strength of individual test pieces from the formula below.

In the case of the particleboards Type 18, Type 13 and Type 8, the smaller value of the bending strengths measured lengthwise and widthwise shall be adopted as the bending strength of the test piece, while for Type 24-10, Type 17.5-10.5 and Type 30-15, the bending strengths in both directions shall be adopted as the bending strength of the test piece.

$$\text{Bending strength } (\text{N/mm}^2) = \frac{3PL}{2bt^2}$$

where, P: maximum load (N)
L: span (mm)
b: width of test piece (mm)
t: thickness of test piece (mm)

Unit : mm

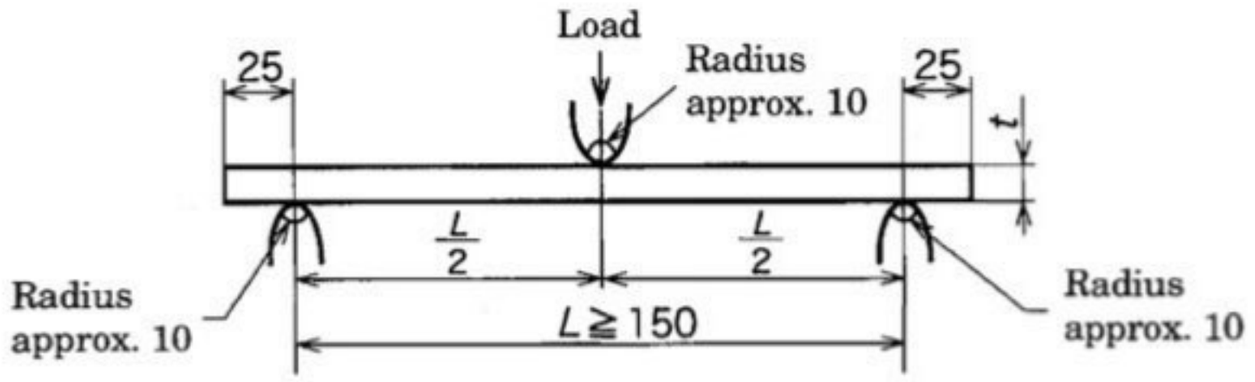

Fig. 6 Test apparatus of bending strength

6.6 Bending strength test under wet conditions Bending strength test under wet conditions shall be as specified below:

a) **Bending strength test A under wet conditions** Immerse test pieces in warm water of 70 ± 3 °C for 2 h, and after further immersing them in water of ordinary temperature for 1 h, carry out the bending strength test specified in **6.5** as they are still wet. Calculate the bending strength under wet conditions of individual test pieces.

In the case of the particleboards Type 18 and Type 13, the smaller value of the bending strengths measured lengthwise and widthwise shall be adopted as the bending strength of the test piece, while for Type 24-10, Type 17.5-10.5 and Type 30-15, the bending strengths in both directions shall be adopted as the bending strength of the test piece. In calculating the bending strength under wet conditions, the dimensions of the test pieces before immersion shall be adopted.

b) **Bending strength test B under wet conditions** Immerse test pieces in boiling water for 2 h, and after further immersing them in water of ordinary temperature for 1 h, carry out the bending strength test specified in **6.5** as they are still wet. Calculate the bending strength under wet conditions of individual test pieces.

In the case of the particleboards Type 18 and Type 13, the smaller value of the bending strengths measured lengthwise and widthwise shall be adopted as the bending strength of the test piece, while for Type 24-10, Type 17.5-10.5 and Type 30-15, the bending strengths in both directions shall be adopted as the bending strength of the test piece. In calculating the bending strength under wet conditions, the dimensions of the test pieces before immersion shall be adopted.

6.7 Test of swelling in thickness after immersion in water Measure the thickness in the centre of a test piece to the nearest 0.05 mm with a dial gauge or a micrometer, and then immerse it in water of 20 ± 1 °C horizontally about 3 cm below the water surface for 24 h, take it out, wipe off the water and measure the thickness again in the same manner as above. Calculate the swelling in thickness after immersion in water from the formula below:

$$\text{Swelling in thickness after immersion in water (\%)} = \frac{t_2 - t_1}{t_1} \times 100$$

where, t_1 : thickness (mm) before immersion in water

t_2 : thickness (mm) after immersion in water

6.8 Internal bond test Adhere a test piece to steel or aluminum blocks shown in Fig. 7, apply a tension load vertically to the board face, measure the maximum load (P') at the time of failing force (breaking load of perpendicular tensile strength to the board), and calculate the internal bond from the formula below.

In this test, the tension loading speed shall be approximately 2 mm/min.

$$\text{Internal bond (N/mm}^2\text{)} = \frac{P'}{2bL}$$

where, P' : maximum load (N) at the time of failing force
b : width (mm) of sample
L : length (mm) of sample

Unit : mm

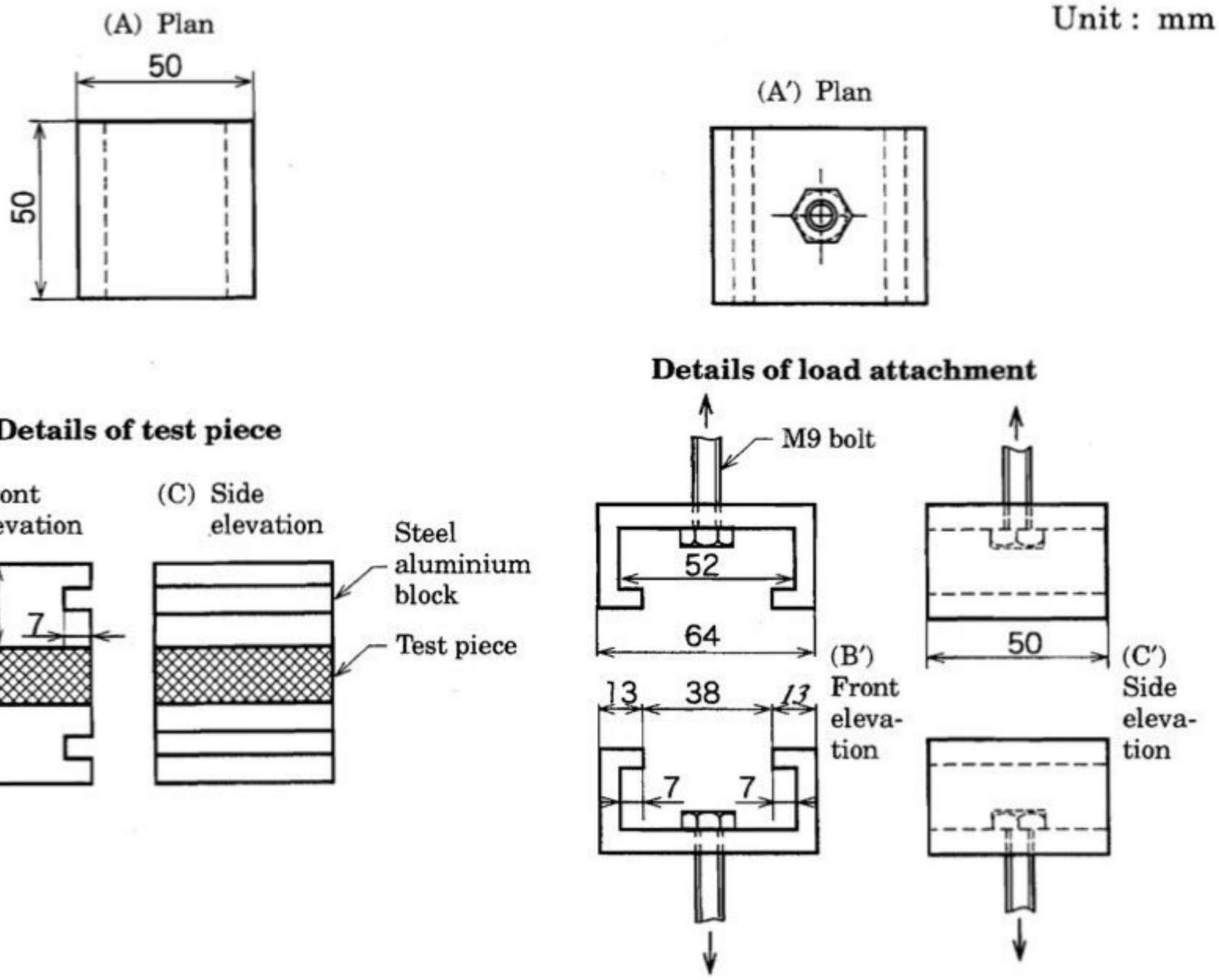

Information : For the adhesion of the steel or aluminium block to the test piece, it is preferable to use an epoxy series resin or hot melt adhesive.

Fig. 7 Test apparatus of internal bond

6.9 Test of wood screw holding power Screw in(12) the threaded part (approximately 11 mm) of the wood screw of 2.7 mm in nominal diameter and 16 mm in nominal length specified in **JIS B 1112**, into the two positions in test pieces vertically as shown in Fig. 8, pull out the screws vertically after fixing the test piece, measure the maximum loads required for pulling out, and consider the mean value of the two operations the wood screw holding power. In this test, the pulling-out load speed shall be approximately 2 mm/min.

Note (12) Guide holes of about 3 mm deep should be made by using a drill of 2 mm in diameter.

Unit : mm

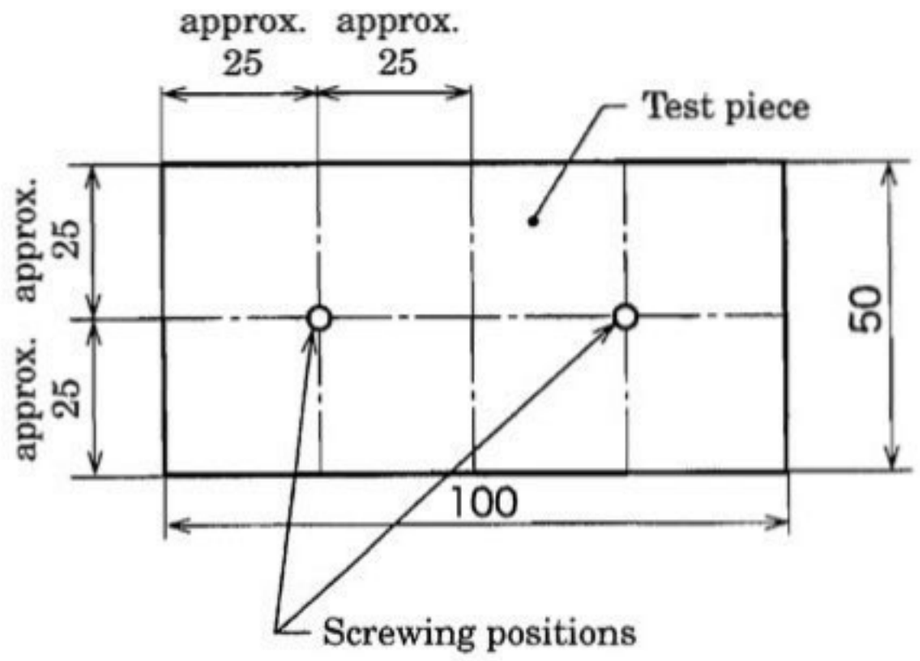

Fig. 8 Test piece for wood screw holding power

6.10 Formaldehyde emission test The formaldehyde emission test shall be carried out on the three boards sampled respectively according to **JIS A 1460**, and the mean value and the maximum value of them shall be regarded as the emission quantity. However, the measured value for two sets of test piece in one sheet of board shall be expressed by two places of significant figure, and the mean value shall be rounded-off to one place of decimal. The mean value of measured values for three boards shall be, also, rounded-off to one place of decimal.

The method to round-off numeral value shall be in accordance with **JIS Z 8401**.

6.11 In-plane tensile strength test Adhere to the centre of the surface of test piece the attachment having the adhering surface of a square whose side is 20 mm or of a circle whose area is 400 mm^2 by using the adhesive, make a notch of the depth to reach the substrate around the attachment after the adhesive is hardened, fix the test piece and the attachment as shown in Fig. 9, pull them at the load speed of about 2 mm/min in the direction orthogonal to the adhering surface, measure the maximum load (P') at the time of failing force, and calculate the in-plane tensile strength by the formula below:

$$\text{In-plane tensile strength (N/mm}^2) = \frac{P'}{400}$$

where, P' : maximum load (N) at the time of failing force

400 : area (mm^2) of adhered attachment

Unit : mm

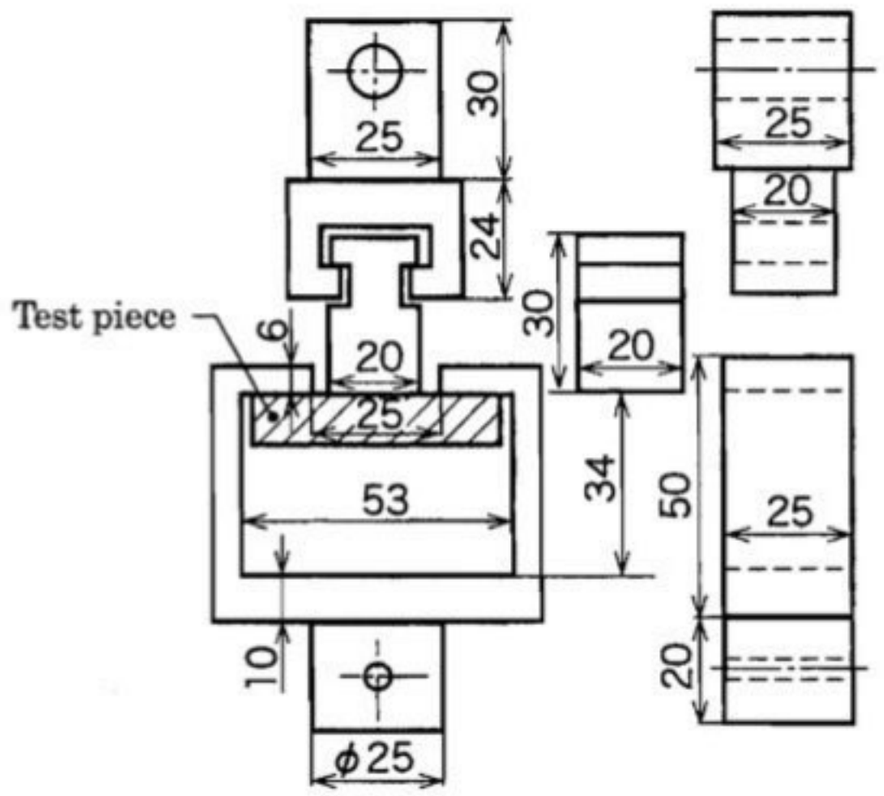

Test piece for in-plane tensile strength

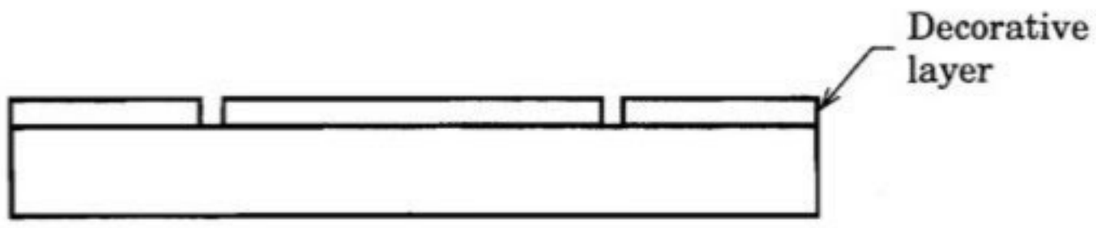

Fig. 9 Test piece for in-plane tensile strength test and attachment

6.12 Impact resistance test Place the test piece of the impact resistance test with its surface upside by the full-support method on the sand as specified in S1 of Table 3 of **5.2** of **JIS A 1408**, and drop a spherical weight made of iron and steel as specified in Table 15 onto the centre part of the surface from the prescribed height. Visually observe cracks or fractures on the surface and measure the diameter of the recess.

Table 15 Weight to be used in impact resistance test

Thickness of test piece mm	Weight to be used				Falling height of weight cm
	Symbol	Mass g	Nominal size	Diameter mm	
Under 15	W_2-300	Approx. 286	$1\frac{5}{8}$	Approx. 41	50
15 or over	W_2-500	Approx. 530	2	Approx. 51	100

6.13 Acid resistance test Place the test piece horizontally, add several drops of 5 % acetic acid solution(13) onto the surface, cover the dropped part by a watch glass, and after 2 h, remove the watch glass and immediately wash the surface with water, leave it alone in a room, and visually observe the surface condition after 24 h.

Note (13) The acetic acid solution shall be prepared by using acetic acid as specified in **JIS K 8355** or acetic anhydride as specified in **JIS K 8886**.

6.14 Alkali resistance test Place the test piece horizontally, add several drops of 1 % sodium carbonate solution(14) onto the surface, cover the dropped part by a watch glass, and after 2 h, remove the watch glass and immediately wash the surface with water, leave it alone in a room, and visually observe the surface condition after 24 h.

Note (14) The sodium carbonate solution shall be prepared by using sodium carbonate (10 hydrate) as specified in **JIS K 8624** or sodium carbonate as specified in **JIS K 8625**.

6.15 Stain resistance test Fix the test piece horizontally, place a plate having punched hole parts of 2 cm × 4 cm on the surface thereagainst, and paint the whole surface of the test piece until no decorative surface is found by using a crayon (red) specified in **JIS S 6026**. After leaving alone for 2 h, remove the crayon so as not to damage the decorative layer by a cloth or a nylon brush containing petroleum benzine specified in **JIS K 8594**, and observe it by using a grey scale specified in **JIS L 0805**.

6.16 Change-in-colour resistance test After irradiation for 48 h in accordance with B-1 method of **2** (**2.1**) of **JIS K 7102** by using a testing machine specified in **3.1** (**1**) of **JIS K 7102**, visually observe cracks, swells or the like on the surface. Then, leave it alone in a dark place in a relative dry room.

The reference test piece which is not irradiated shall previously be left alone in the same place.

In 2 h or more after irradiation, take the test piece out of the dark place, and measure the change-in-colour by using a grey scale as specified in **JIS L 0804**, or measure the change-in-colour based on the method of $L^*a^*b^*$ colour system as specified in **JIS Z 8730** by using a colorimeter as specified in **JIS K 7102**. However, the change-in-colour shall be judged by the mean value of three colour difference values for the test pieces with graining or other patterns.

Remarks : When a light-and water-exposure apparatus (enclosed carbon-arc type) or a light-and water-exposure apparatus (open-flame sunshine carbon-arc type) is use, the comparative data after irradiation of 48 h of a light-exposure apparatus (enclosed carbon-arc type) shall be confirmed.

6.17 Scratch resistance test Slide the test piece with its surface upside for about 30 mm lengthwise and widthwise by using a scratch tester of Martens type where the diameter of the sphere is 3 mm and the load of the tester is 4.9 N. Carry out the test at three points both lengthwise and widthwise, and then, visually observe the test piece from the position of about 60 cm apart.

6.18 Thermal insulation test The thermal insulation test shall be made in accordance with **JIS A 1420**, the thermal resistance shall be obtained at the time when the surface temperature is measured at mean temperature of 30 ± 3 °C in the state of upward heat flow direction.

6.19 Incombustibility test The incombustibility test shall be made in accordance with **JIS A 1321**.

7 Inspection The inspection shall be as follows:

a) The shape, dimensions, appearance and quality shall be inspected by a reasonable inspection method.

b) The emission quantity of formaldehyde, thermal insulation, acid resistance, alkali resistance, stain resistance, change-in-colour resistance, scratch resistance and incombustibility shall be inspected by the type inspection when the product is newly designed or modified, or when the conditions of production are changed.

8 Designation Designation of the particleboards shall be as specified in the following examples. However, unnecessary items such as the classification according to the face and back, according to the bending strength of the veneered particleboard, and according to the incombustibility may be omitted.

Example 1 Base-unpolished 13 U F☆☆☆☆ Regular Particleboard

RN-13UF☆☆☆☆ Regular-P
or 13UF☆☆☆☆-PB

- Regular — Classification according to the incombustibility
- F☆☆☆☆ — Symbol of classification according to the formaldehyde emission quantity
- U — Classification according to the adhesive
- 13 — Classification according to the bending strength
- Base-unpolished — Classification according to the surface condition

Example 2 Base-polished 18PF☆☆☆ Incombustibility grade 2 Particleboard

RS18PF☆☆☆ Incombustibility grade 2-PB
or 18PF☆☆☆ Incombustibility grade 2-PB

Example 3 Veneered-unpolished 35-15F☆☆ Regular particleboard VNMF☆☆-PB

Example 4 Plastics overlay 13MF☆☆☆☆ Decorative particleboard

DO13MF☆☆☆☆-PB

9 Marking Particleboards shall be marked with the items enumerated below on each product or on each package.

Moreover, for the products for floor substrates, roof substrates, inner and outer wall substrates, the items of the kind (or symbol) of classification according to formaldehyde emission quantity, **c**) and **d**) shall be marked for each product.

a) Classification or symbol

b) Dimensions (thickness × width × length)

c) Year and month of manufacture or their abbreviation

d) Name of manufacturer or its abbreviation

e) Cautions

Example : Care shall be enough taken of storage because of being in danger of absorbing formaldehyde emitted from other products.

Attached Table 1 Normative references

JIS A 1321	*Testing method for incombustibility of internal finish material and procedure of buildings*
JIS A 1408	*Test methods of bending and impact for building boards*
JIS A 1420	*Determination of steady-state thermal transmission properties—Hot box method*
JIS A 1460	*Building boards determination of formaldehyde emission—Desiccator method*
JIS B 1112	*Cross-recessed head wood screws*
JIS B 7526	*Squares*
JIS K 7102	*Testing method for colour fastness of plastics upon exposure to light of the carbon arc*
JIS K 8355	*Acetic acid*
JIS K 8594	*Petroleum benzine*
JIS K 8624	*Sodium carbonate decahydrate*
JIS K 8625	*Sodium carbonate*
JIS K 8886	*Acetic anhydride*
JIS L 0804	*Grey scale for assessing change in colour*
JIS L 0805	*Grey scale for assessing staining*
JIS S 6026	*Crayons and oil pastels*
JIS Z 8401	*Guide to the rounding of numbers*
JIS Z 8730	*Colour specification—Colour differences of object colours*

Errata for JIS (English edition) are printed in *Standardization Journal*, published monthly by the Japanese Standards Association, and also provided to subscribers of JIS (English edition) in *Monthly Information*.

Errata will be provided upon request, please contact:

Standardization Promotion Department, Japanese Standards Association
4-1-24, Akasaka, Minato-ku, Tokyo, 107-8440 JAPAN
TEL. 03-3583-8002 FAX. 03-3583-0462

coatings

MDPI

Article

Highly Hydrophobic Organic Coatings Based on Organopolysilazanes and Silica Nanoparticles: Evaluation of Environmental Degradation

Lucía Pérez-Gandarillas *, Daniel Aragón, Carmen Manteca, Marina Gonzalez-Barriuso, Laura Soriano, Abraham Casas and Angel Yedra

Centro Tecnológico de Componentes-CTC, Scientific and Technological Park of Cantabria (PCTCAN), 39011 Santander, Spain

* Correspondence: lperez@centrotecnologicoctc.com

Abstract: Hydrophobic coatings have potential applications in various fields, including for corrosion and weathering protection. In this study, we investigated the use of organopolysilazanes (OPSZs) combined with hydrophobic nanoparticles (NPs) on steel as a substrate to obtain hydrophobic coatings. The coatings were characterized using various techniques, and their hydrophobic properties and corrosion and weathering resistance were evaluated under near-shore marine conditions with high salinity, humidity and UV radiation. Our results show that the coatings exhibited excellent hydrophobic properties and significantly improved corrosion and weathering resistance compared to an uncoated steel and a pristine polymer. These findings suggest that the developed coatings have the potential to provide protection against corrosion for atmospheric and splash exposures in marine environments.

Keywords: hydrophobicity; hydrophobic coatings; organopolysilazanes; hydrophobic nanoparticles; corrosion resistance; environmental degradation

Citation: Pérez-Gandarillas, L.; Aragón, D.; Manteca, C.; Gonzalez-Barriuso, M.; Soriano, L.; Casas, A.; Yedra, A. Highly Hydrophobic Organic Coatings Based on Organopolysilazanes and Silica Nanoparticles: Evaluation of Environmental Degradation. *Coatings* **2023**, *13*, 537. https://doi.org/10.3390/coatings13030537

Academic Editor: Ioannis Karapanagiotis

Received: 23 January 2023
Revised: 22 February 2023
Accepted: 22 February 2023
Published: 1 March 2023

1. Introduction

Surface wetting behavior can generally be classified into four different regimes based on the value of the water contact angle (WCA, θ): superhydrophilic (θ < 10°), hydrophilic (10° < θ < 90°), hydrophobic (90° < θ <150°), and superhydrophobic (θ > 150°) regimes [1,2]. Studies have demonstrated that an adequate combination of surface roughness and chemical composition is the key for the preparation of hydrophobic and superhydrophobic engineered surfaces.

Hydrophobic and superhydrophobic surfaces have aroused great attention among the scientific and industrial communities for their high water repellence, which entails associated properties of interest, such as anti-corrosion, self-cleaning, anti-icing, anti-adherence, reduction of bio-fouling, and antimicrobial or water vapor barrier effects, among others [1,2]. Therefore, these surfaces offer a wide range of technological applications for diverse sectors.

Various materials and techniques have been used to prepare hydrophobic and superhydrophobic coatings, including both organic and inorganic materials, as well as diverse techniques, such as electrochemical deposition [3], sol–gel [4,5], plasma etching [6], chemical vapor deposition [7], templating, etching, anodization, self-assembling, dip-coating and spray-coating techniques [8–10]. These methods can result in different morphologies, roughnesses, and chemical compositions of the coatings, which impact their water-repellent properties [10]. However, the main limitation of most of the employed methods is their high cost, associated with their application complexity or the amount of processing required to accurately create nanostructures. In addition, since hydrophobicity is a superficial property, the main disadvantage is its limited durability against degradation by external agents.

Hydrophobic surfaces can be deteriorated by several environmental mechanisms, mainly by mechanical wear, although others, such as chemical reactions with solvents or gases, ultraviolet (UV) exposure, rain, humidity and contamination, also contribute [11].

The vast majority of hydrophobic and superhydrophobic surfaces have a very limited resistance to abrasion and environmental degradation (losing hydrophobicity at the outermost layer), and, therefore, the stability of the nanocoating has a reduced durability [1,12]. The challenge of durability has restricted the use of hydrophobic surfaces in commercial and industrial applications [11].

In order to overcome the aforementioned limitations, the use of nanotechnology for the formulation of new durable and effective hydrophobic coatings is postulated as a potential solution. Polymer-based nanocomposites are one of the most popular fields of current research. Specifically, nanocomposite fabrication from organic polymers using nanoparticles as additives has been creating high expectations in the coatings industry sector [13].

Organic nanocomposite coatings consist of a polymeric matrix to which a nanofiller is integrated, which provides the intended functionality to the surface. The great advantages of organic coatings over other types of coatings are the abilities to obtain excellent properties at a lower cost and to use simple application technologies.

However, due to the high specific surface of nanomaterials, the tendency to aggregate means that their integration into polymeric matrices is still a technically complex process. In this sense, in order to achieve the characteristic of hydrophobicity and, at the same time, durability over time, it is necessary to guarantee an optimal integration of the nanomaterials in the polymeric matrix.

Different authors have carried out studies to obtain hydrophobic paints based on nanotechnology [14–16]. Unfortunately, in general, the polymeric matrices surround the integrated hydrophobic nanoparticles, inhibiting their hydrophobic character (Figure 1a). Therefore, improving nanoparticle–polymer and coating–substrate interfacial adhesions may be the key to improving the durability of hydrophobic coatings. The use of a polymer as an anchor binder that acts as a film-forming agent can (i) avoid the inhibition of the hydrophobic functionality of nanoparticles and (ii) ensure the adhesion of nanoparticles to the substrate (Figure 1b).

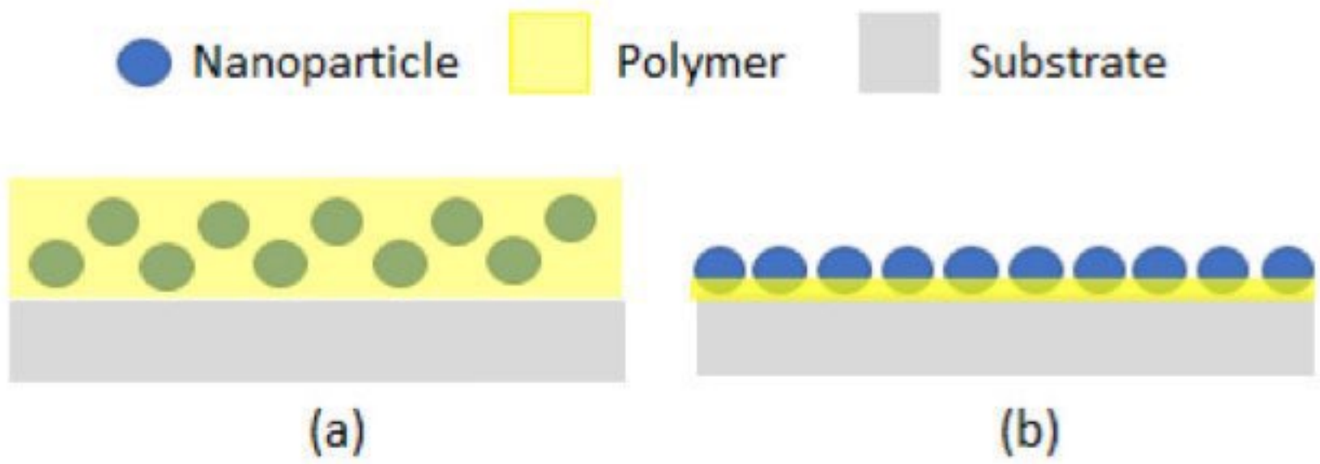

Figure 1. Schematic illustration of nanoparticle integration: (**a**) complete embedment of nanoparticles in the polymer; (**b**) polymer acting as bonding layer between nanoparticles and substrate.

The scientific community is searching for high-strength polymeric matrices, and, in this context, polysilazanes are attracting attention due to their extraordinary properties [17]. Polysilazanes (PSZs) are a class of special polymers with a structure containing alternating nitrogen and silicon atoms: —$(SiR^1R^2—NR^3)_n$—. These polymers can be converted to ceramics at approximately 1000 °C and have been widely used as precursors for silicon carbonitrides [18–20].

In particular, organopolysilazanes (OPSZs) are PSZs that bond to carbon atoms. The high reactivities of the Si-H and N-H groups present in the structures of OPSZs form a very dense silica network, notably improving adherence to different substrates (glass, plastic, metal, etc.) [21]. OPSZs are highly crosslinked, combine good barrier properties

and exhibit a high mechanical strength and a strong affinity with metallic substrates. In addition, recently, OPSZs have been developed to rapidly cure at room temperature by interacting with ambient moisture, which has generated considerable interest in simplifying the curing process. These types of polymers are used in various sectors for high-value-added applications, such as electronics. In terms of corrosion resistance, their good barrier properties have been proven [21–23].

There are studies in the scientific literature that use this type of polymer for hydrophobicity applications [24,25]. However, research in this field has shown that the hydrophobicity values achieved using organopolysilazanes (in the range between a 90° and 95° water contact angle) are far from those of superhydrophobicity. In most of the studies carried out, the OPSZ is applied pure mainly on aluminum due to its adhesion capacity, which prevails over hydrophobicity [26]. Therefore, there is scarce literature on its use on other substrates with greater application, such as steel [21,27].

The objective of this work is to study the application of OPSZ combined with hydrophobic nanoparticles on steel as a substrate to obtain highly hydrophobic coatings. Once hydrophobicity is achieved, the durability is tested under near-shore marine conditions with high salinity, humidity and UV radiation. This test allows for the evaluation of how the hydrophobic property favors the corrosion resistance of a coating.

2. Materials and Methods

2.1. Materials

A commercially available OPSZ (Durazane 1500 Rapid Cure) was supplied by Merck KGaA (Darmstadt, Germany). This polysilazane is a low-viscosity liquid, with a high crosslink density and rapid moisture curing at room temperature. As hydrophobic nanoparticles, commercial fumed silica powder, surface-treated with polydimethylsiloxane (Aerosil R202, Evonik Industries AG, Essen, Germany), was used. As solvents, butyl acetate (BAC) and acetone were employed.

For the selection of the solvent and the optimization of the NP percentage, glass substrates were used (76 mm × 26 mm × 1 mm). For the degradation evaluation, standard samples of low-carbon steel (F 6702 according to UNE-36086-1) from Espancolor (Barcelona, Spain) were used as substrates (150 mm × 75 mm × 0.8 mm).

2.2. Methods

2.2.1. Nanoparticle Integration

In order to provide the hydrophobic functionality to the coating, different amounts of nanoparticles were mixed with the OPSZ polymer. Firstly, the hydrophobic silica nanoparticles were dispersed in the solvent by using ultrasound for 15 min (Sonopuls HD3200, Bandelin, Berlin, Germany). To this solution, different amounts of OPSZs were added, and the nanoparticles were integrated via mechanical stirring into the polymer in a range between 0% and 50% of the mass of the polymer. The OPSZ worked as a binder to anchor the nanoparticles to the substrate.

2.2.2. Sample Preparation

For the deposition of the coatings on steel substrates, two different techniques were used in order to compare their effects on the final properties of the coating. On the one hand, spray-coating deposition was carried out using a compressed dry air spray gun (Mini Xtreme, Sagola, Vitoria, Spain), operating at a pressure of 2 bars. The spray technique has the advantages of being able to carry out coatings both on a large scale and of irregular parts and at a low price. On the other hand, the dip-coating technique is adequate for the synthesis of thin layers, has the advantage of simplicity and the possibility of adjusting the parameters to obtain more precise coatings. According to our own expertise, the following conditions of the dip coater (ND-DC 11/1, Nadetech Innovations, Noain, Spain) were selected: 100 mm/min for the immersion rate and 30 mm/min for the emersion rate.

A preliminary evaluation of the formulations with different percentages of NPs was carried out by depositing the coatings on glass substrates via dip coating. Then, an optimum formulation was chosen in terms of hydrophobicity and color variation. With this formulation, steel substrates were coated using both the spray- and dip-coating methods (Figure 2).

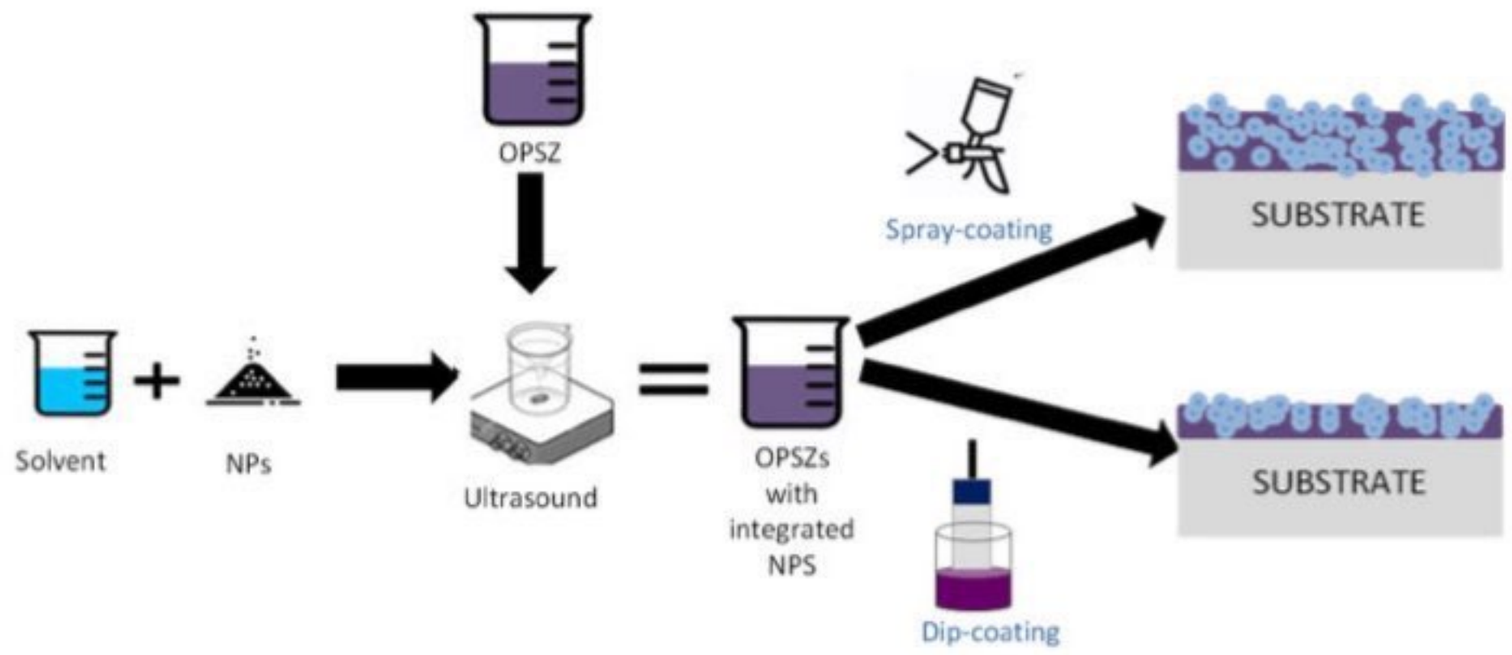

Figure 2. Scheme of the sample preparation process.

Prior to the deposition processes, the steel substrates were washed with ethanol to remove the protective grease. The samples were cured at room temperature for 24 h (T = 20–25 °C; relative humidity = 40%–50%).

2.2.3. Water Contact Angle

The water contact angle (WCA) is a parameter that discriminates the hydrophobic properties of a surface. The contact angle is measured as the angle formed by the line of the surface with the line tangent to the intersections of the modified circumference of a drop. To perform this measurement, an experimental device was prepared consisting of a flat horizontal surface, on which the painted specimen was supported, and a camera was supported on a tripod so that the focus was centered at the same height as the surface of the specimen. Pictures were taken of the water droplets on the substrate and analyzed with the mathematical software GeoGebra [28] to obtain the contact angle (Figure 3). The WCA measurements were performed in triplicate, taking the average and standard deviation of such measurements.

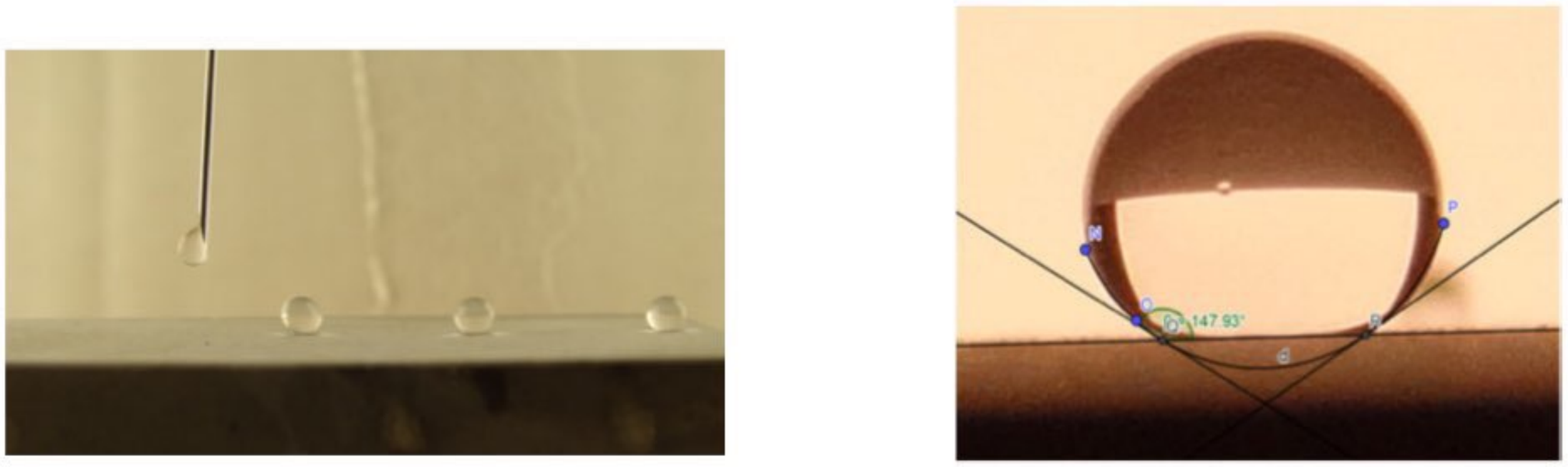

(**a**) (**b**)

Figure 3. (**a**) Water drops rolling off (**b**) Water contact angle measurement.

2.2.4. Coating Thickness

To measure the coating thickness, a portable electronic Positector 6000 (DeFelkco, Ogdensburg, NY, USA) was used. The measurements made by this equipment are fast and non-destructive since it uses magnetic principles and Foucault's current to measure the thickness of the paint on ferrous and non-ferrous metals.

2.2.5. Color Variation

A portable spectrocolorimeter (X-Rite, model RM200QC, Grand Rapids, MI, USA) was used to evaluate the color variation of the coating with respect to the substrate. This equipment can measure the opacity and transparency of a coating through color variation (ΔE). ΔE can be determined from the L^*a^*b color space, also referred to as CIELAB, according to Equation (1):

$$\Delta E = \sqrt{\Delta L^2 + \Delta a^2 + \Delta b^2} \quad (1)$$

where L refers to lightness, a represents red to green coordinates, and b represents coordinates from blue to yellow.

Therefore, ΔE is the numerical comparison between two color samples and indicates the differences in absolute color coordinates. Likewise, the color variation allows for an evaluation of the coating after the degradation tests. According to the literature, if $\Delta E < 5$, color variations are negligible [29]. Color variation was measured in triplicate, taking the average and standard deviation of such measurements.

2.2.6. Environmental Degradation Tests

The specimens obtained were subjected to different degradation tests in order to evaluate their durability.

The corrosion resistance was evaluated through a salt spray test. This test is generally suitable for testing corrosion protection as a quick analysis of discontinuities, pores and damage in organic and inorganic coatings. The salt spray test consists of spraying a sodium chloride solution (5% NaCl) in a controlled environment inside a salt spray chamber (Dycometal, model SSC400, Barcelona, Spain) where the specimens are located. To carry out this test, the ISO 9227:2017 standard was taken as a reference. Two 24 h cycles were carried out (total time = 48 h) in this work.

The coatings were also exposed to artificial weathering (fluorescent UV lamps and water) with the purpose of simulating the natural aging processes caused by environmental agents, such as sunlight and rain. This test consists of introducing the test pieces into a QUV chamber (Q-Lab, Westlake, OH, USA), where they are exposed to alternating cycles of UV light, condensation and high temperatures, simulating the damage caused by sunlight, rain and dew. This test was carried out, taking the ISO 11507:2007 standard as a reference, during a 120 h cycle with alternate cycles of sprayed water and UV light and an inspection every 24 h.

The resistance of the coatings to environmental degradation was evaluated by measuring the contact angle and color variation before and after the degradation tests (Figure 4).

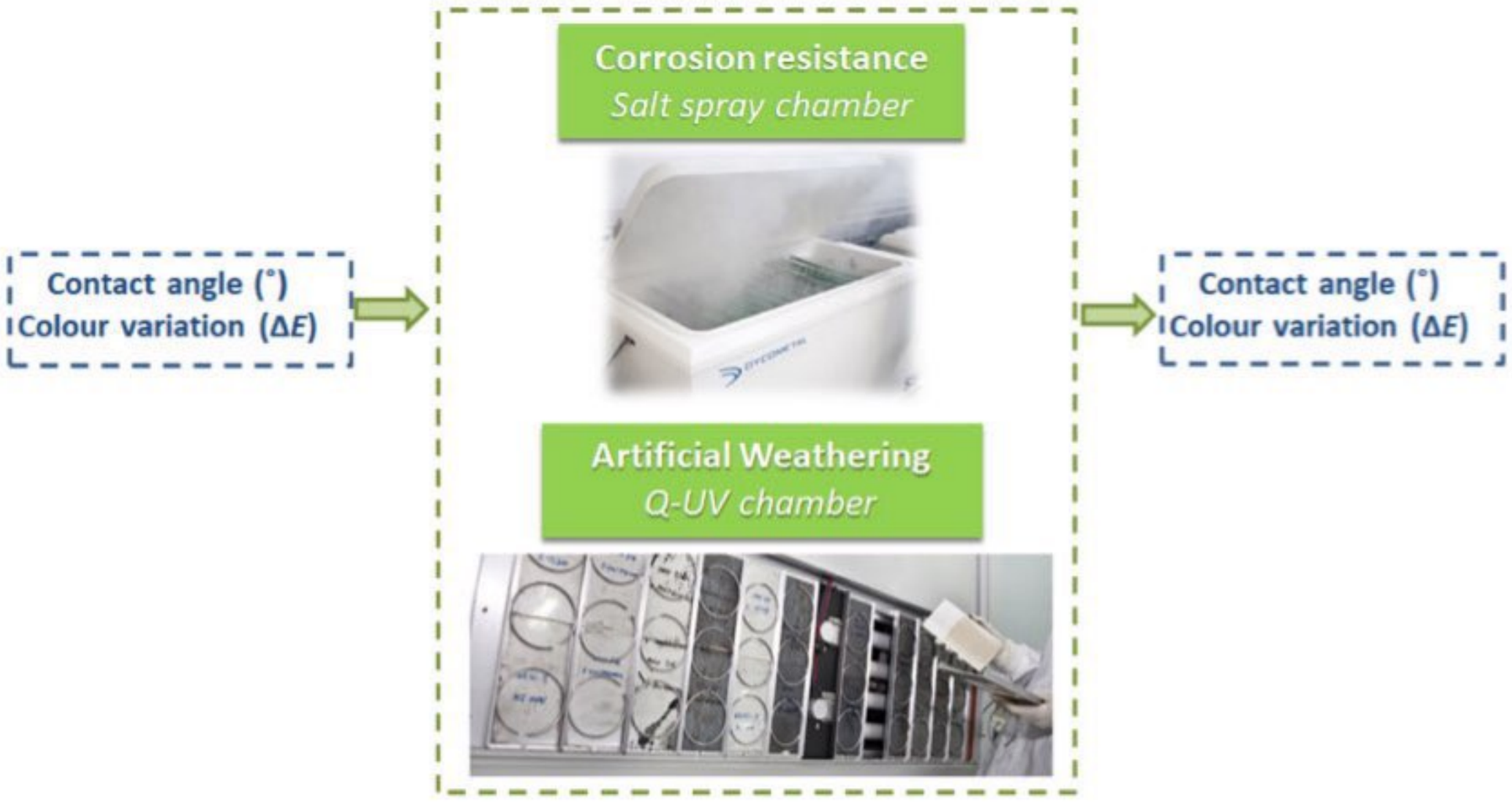

Figure 4. Environmental degradation tests conducted to evaluate the durability of coatings.

2.2.7. Electrochemical Impedance Spectroscopy (EIS)

Electrochemical Impedance Spectroscopy (EIS) measurements were performed on the developed samples. EIS is an electrochemical technique usually utilized for evaluating the corrosion behavior of coatings and provides insights into the corrosion reaction of a substrate [30]. An evaluation of the impedance of a coated system as a function of frequency supplies useful information regarding the barrier properties of the coating, the corrosion susceptibility of the substrate and the interfacial layer [31].

EIS tests were performed on an Autolab PGSTAT204N potentiostat, (Metrohm Hispania, Madrid, Spain) with the Nova 2.1 software version for analyses. A three-electrode corrosion cell was used with the coated samples as a working electrode, a platinum wire as a counter electrode, a Ag/AgCl (3.5 M KCl) as a reference electrode and the samples being tested as working electrodes. A 5 wt% sodium chloride solution in deionized water was used as the electrolyte. The coating exposure area for testing was 12.6 cm^2, corresponding to a circular area of 4 cm in diameter. The tests were conducted under stagnant conditions at room temperature (20–25 °C) and were performed on two coated replicas per system inside a Faraday cage. For this study, the sweep conditions for running the EIS tests were carried out over a frequency range from 100 kHz to 0.01 Hz with 7 readings per decade of frequency at 20 mVRMS amplitude sinusoidal perturbation with respect to the open-circuit potential.

3. Results and Discussion

3.1. Selection of Solvent

In order to use the minimum amount of nanoparticles necessary to achieve hydrophobicity, it is necessary to first dilute polysilazane in a solvent. The selection of a proper solvent for polymer dissolution is important to guarantee good nanoparticle dispersion and the durability of the coating. According to the technical datasheet, the Durazane 1500 Rapid Cure Resin reacts in the presence of water, steam or alcohols, so it is important to use solvents with the lowest possible water content. Organic solvents, such as alkanes, esters, ethers, aromatics and ketones, are chemically compatible with the resin. After consultation with the polymer manufacturer, two potential solvents were selected based on their availability/price ratio: butyl acetate (BAC) and acetone.

For the evaluation of which of the two solvents works better, different solutions with different percentages of OPSZs were prepared via mechanical stirring using each type of solvent (BAC and acetone).

It was found that, in both cases, the viscosity was lower than that of the original polymer and that there was no problem in spray painting or dip coating. However, color degradation (yellowing) over time was observed in the formulations where acetone was used. Therefore, BAC was selected for the development of the formulations.

3.2. Evaluation of Optimum Percentage of Nanoparticles

Different ratios of OPSZ:NPs (the percentage of NPS varied from 0% to 50%) were used and deposited in glass samples via dip coating (Figure 5). It can be observed that, when the percentage of NPs in the formulation increases, the coating becomes whiter and opaquer.

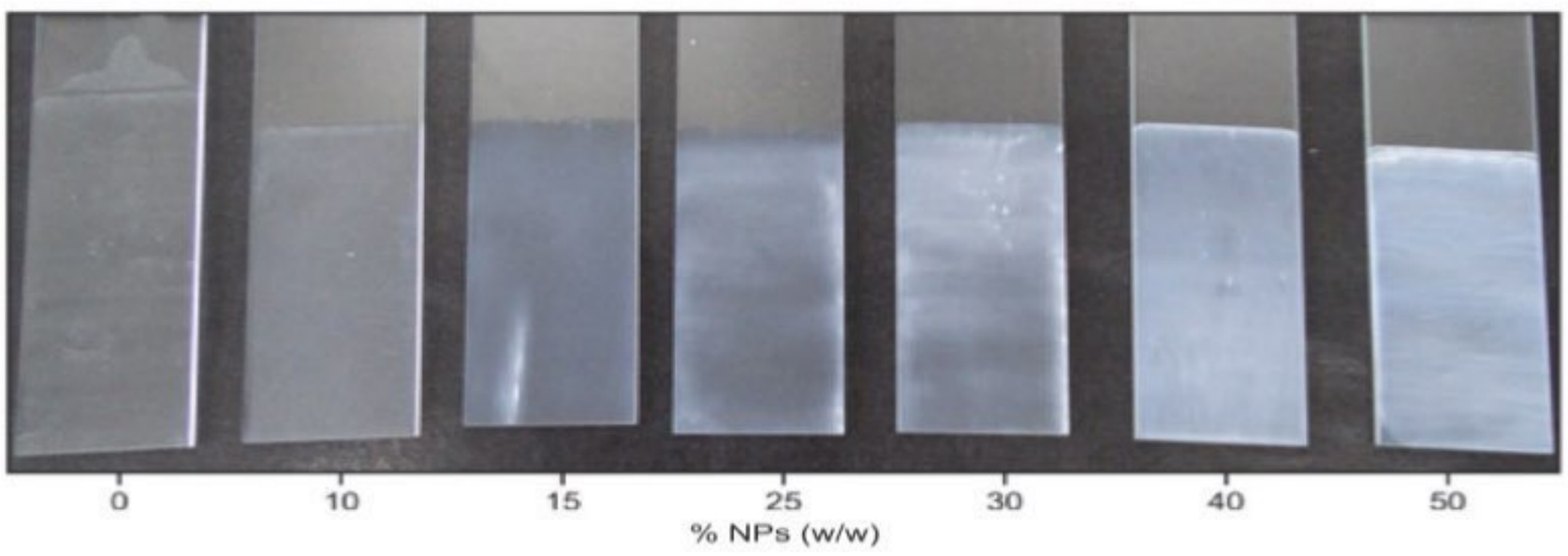

Figure 5. Glass samples coated with several ratios of OPSZ/NPs.

Then, the WCA and the color variation were measured in these samples and are presented in Figures 6 and 7.

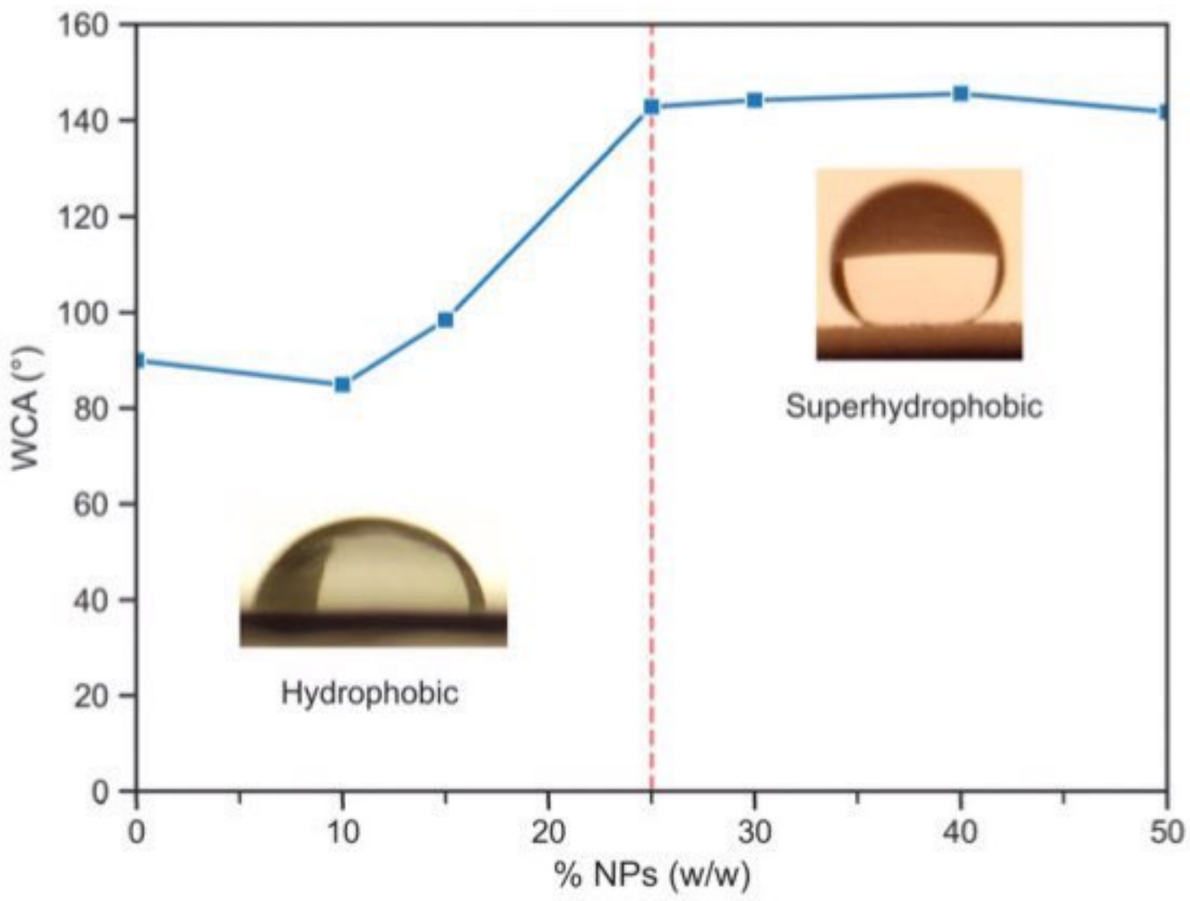

Figure 6. WCA in a flat surface for different concentrations of NPs.

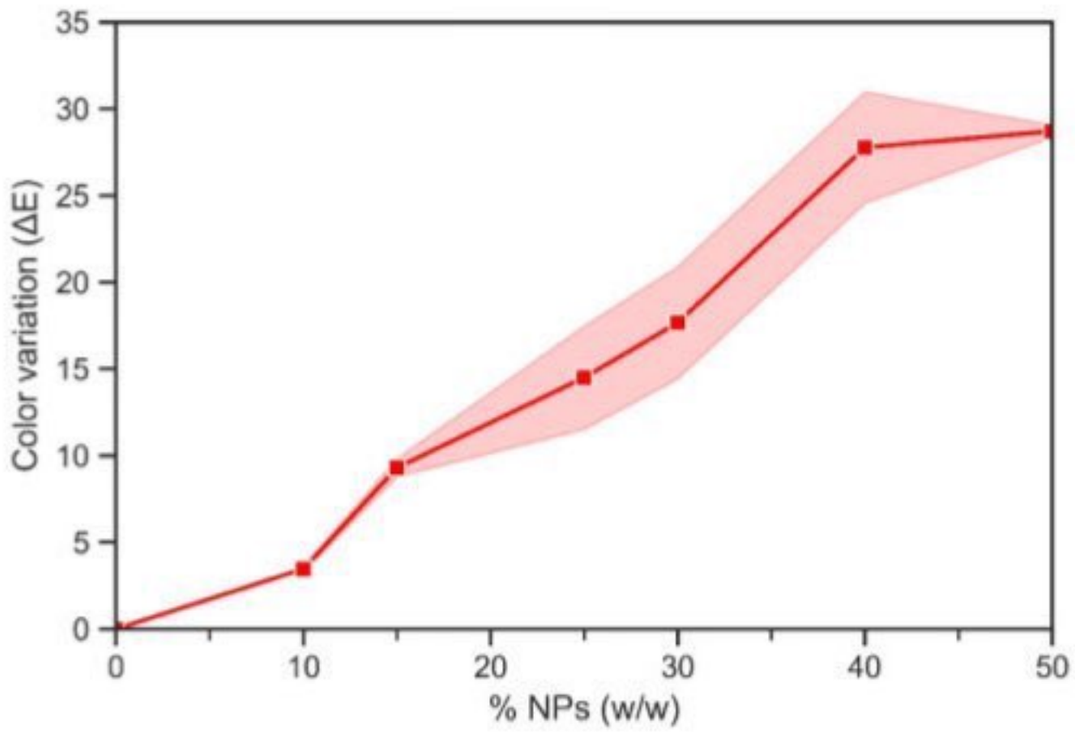

Figure 7. Color variation (ΔE) for different concentrations of NPs (shadowed area corresponds to the standard deviation).

The data presented in Figure 6 clearly illustrate a correlation between the WCA and the NP content. As shown, the maximum WCA is achieved when the NP content is increased up to 25%. Beyond this point, the WCA remains constant. The resulting WCA indicates a highly hydrophobic behavior, very close to the superhydrophobic regime.

The correlation between the WCA and nanoparticle concentration has already been observed by other authors [32–35]. It could be explained by the Cassie–Baxter model because a suitable and optimal hydrophobic NP integration into resin promotes the formation of a micro- and nano-roughness surface, where air trapping takes place [1,11]. These air pockets significantly increase hydrophobicity.

Regarding the color variation, it increases when the percentage of NPs in the formulation increases. It is obvious that the NPs contribute to the changing color of the polymers, because they act like white pigments.

According to the WCA results, the chosen proportion of OPSZ:NPs is 75:25. With this ratio, hydrophobicity is achieved, while the color variation is maintained as minimum as possible. With higher percentages of NPs, hydrophobicity is not improved, while the coatings become whiter.

Therefore, with a 75:25 proportion of OPSZ:NPs, a bench test of the samples is carried out using the spray- and dip-coating techniques. The main characteristics of the obtained samples are shown in Table 1.

As can be seen in the pictures included in Table 1, the samples obtained via dip coating are more homogeneous than the ones obtained via spraying, and the thickness is much lower. Moreover, the dip-coated samples have less color variation than the sprayed samples. This is directly related to the reduced thickness (5 μm) that is obtained via dip coating. A lower thickness implies less color variation.

It can also be observed that the quality of the sprayed coating is not good and that surface defects appear on the surface. These surface defects are attributed to the deposition method. During the spraying process, a rapid evaporation of the solvent takes place, and, therefore, the nanoparticles are not wet enough when reaching the substrate surface. The Si-N bonds present in the polysilazane structure react with the moisture present in the air without being deposited on the substrate, thus producing cyclotetrasiloxanes [36], which are solid at room temperature.

Table 1. Main characteristics of the studied coatings.

Formulation	Thickness (μm)	ΔE	WCA (°)	Appearance (Dimensions 150 × 75 mm)
OPSZ:NPs 100:0 (control sample obtained via spray coating)	29 ± 1	-	90 ± 2	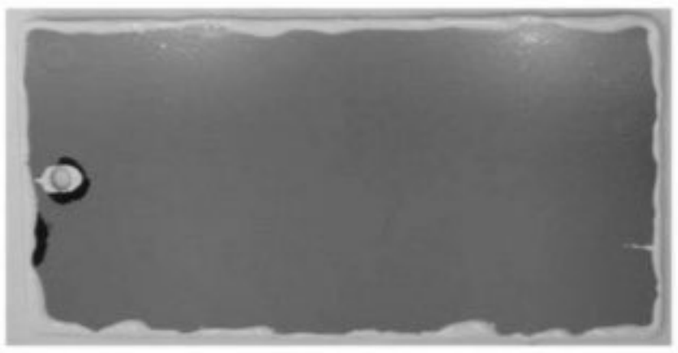
OPSZ:NPs 75:25 Spray coating	63 ± 10	17 ± 1	147 ± 1	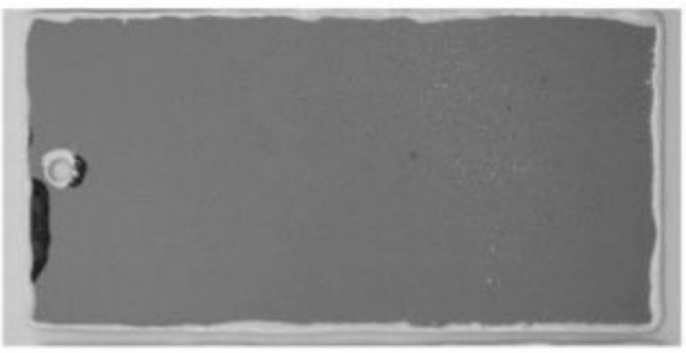
OPSZ:NPs 75:25 Dip coating	5 ± 1	9 ± 1	147 ± 1	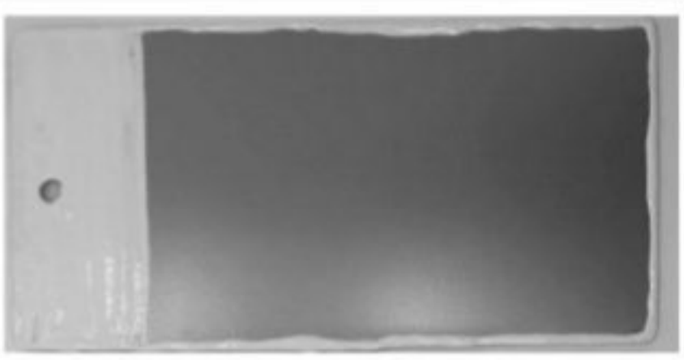

3.3. Salt Spray Test Results

The salt spray test lasted a total of 48 h, although a visual inspection and measurements of the WCA were also carried out after the first 24 h. The pictures taken during the test are included in Figure 8, while Figure 9 shows the evolution of the WCA.

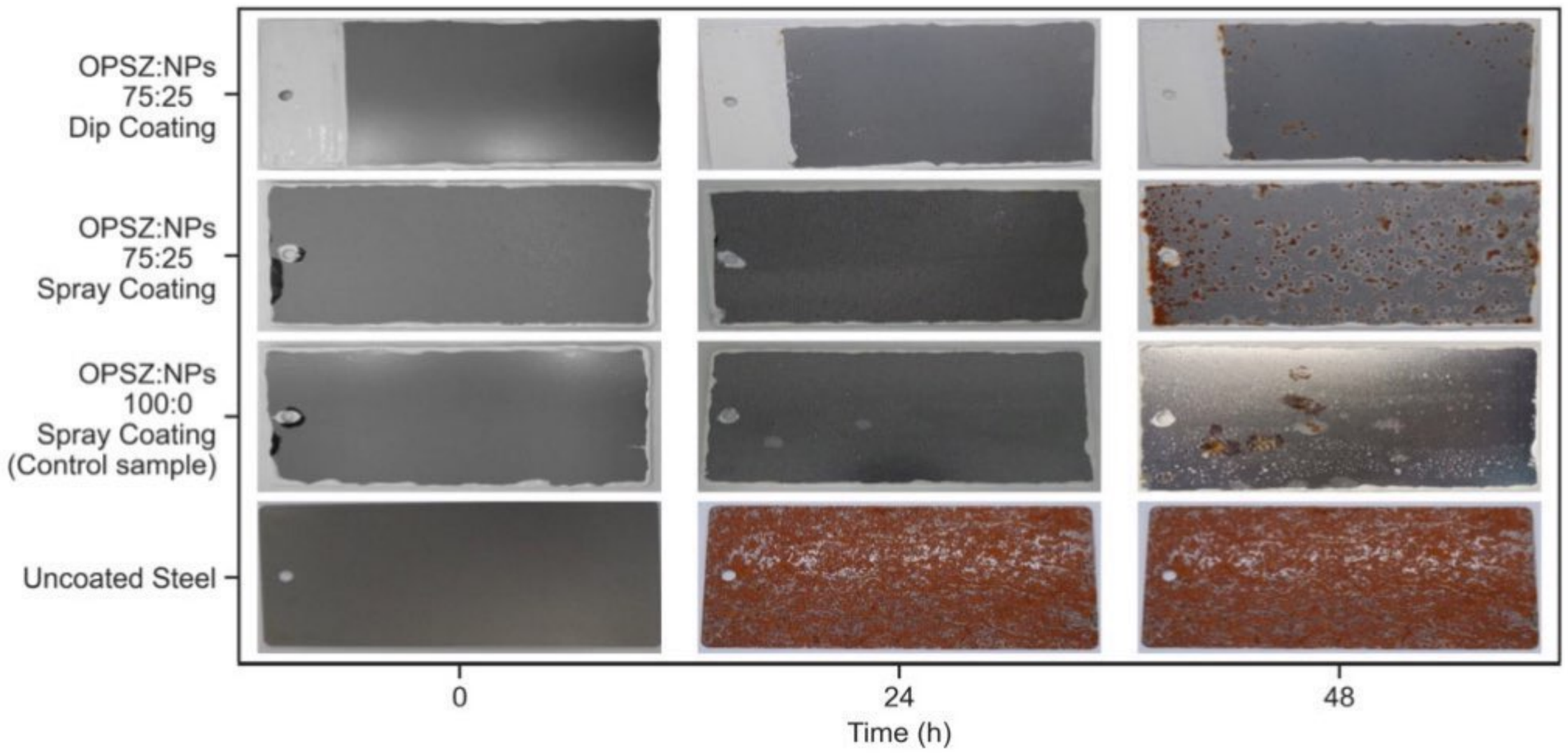

Figure 8. Evolution of coatings on steel during salt spray test.

After 24 h of testing, the three coatings show a greater corrosion resistance than that of bare steel. However, at this time, some pitting is observed in the spray-coated samples with NPs.

At 48 h, in the polymer-based samples (OPSZ:NPs 100:0), salt is deposited on the coatings, although they still resist corrosion. No salt is observed on the coatings that included nanoparticles.

Regarding the samples with the integrated nanoparticles deposited via dip coating, due to their water-repellent character, water deposition is notably reduced in comparison to the control sample. These samples have a greater homogeneity of their finish and, due to this, show a greater resistance to corrosion.

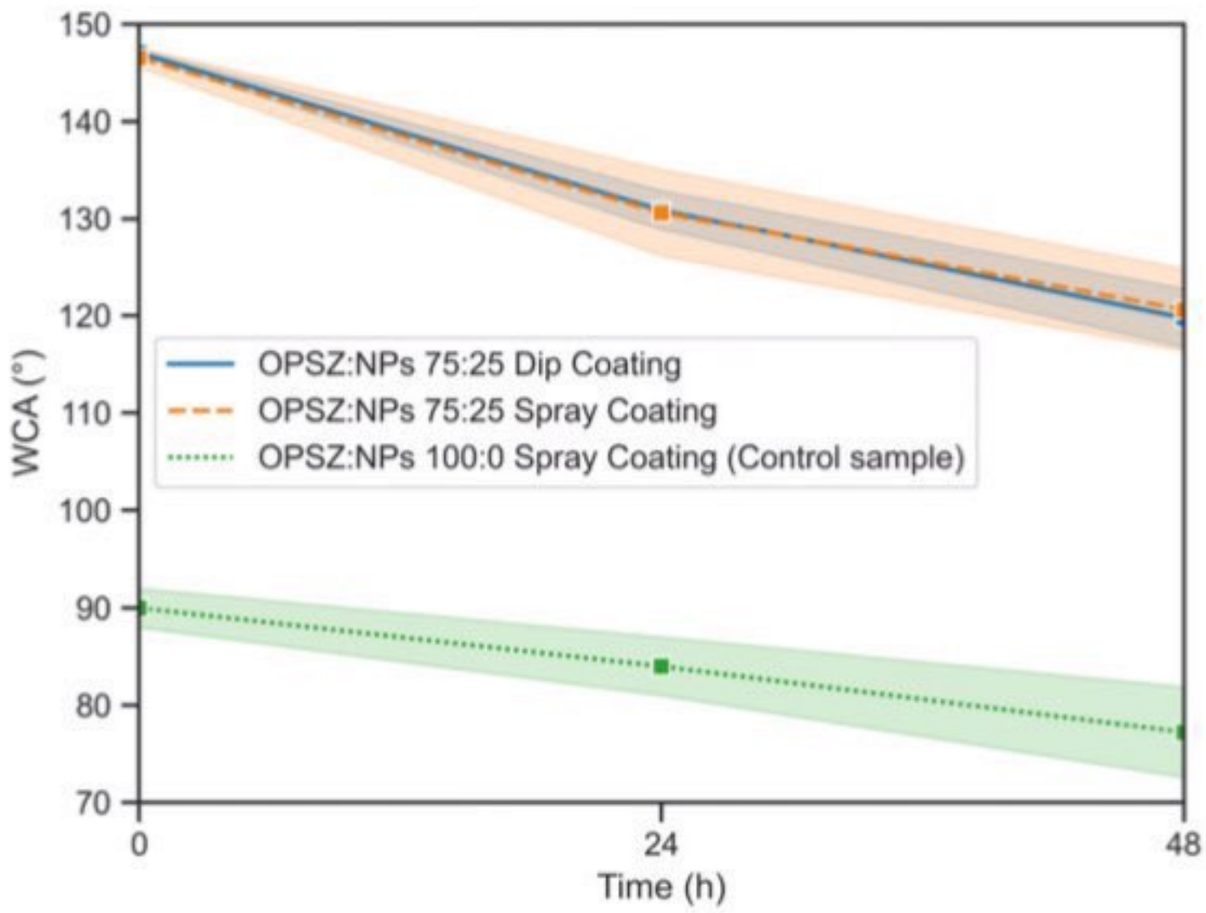

Figure 9. Contact angle measurements versus salt spray test time (shadowed area corresponds to the standard deviation).

On the contrary, in the sprayed coatings (the OPZS:NPs 75:25 spray coating), it can be seen how pitting corrosion begins to appear due to possible imperfections in the finish produced during the spraying process.

Water penetration could not be directly observed in the experiments, but the corrosion in the 75:25 spray-coated sample may be due to the penetration of water through the discontinuities of the surface finish, causing the pitting corrosion phenomenon to take place [37]. Although the control sample is not hydrophobic and droplets of salty water are deposited on the surface, the surface finish is of a higher quality, thus having a lower degree of water penetration, which prevents corrosive species from reaching the metal surface [38]. The defects in the nanocomposite coating deposited via spraying affect the protective function of the coating, which is favorable for the penetration of corrosive media into the film.

The evolution of the contact angle shows a reduction in hydrophobicity over time. However, the values of the WCA obtained for the two deposition methods, spray coating and dip coating, show very similar values. This confirms the fact that the degradation of the spray-deposited samples is due to the bad surface finish and not due to the loss of hydrophobicity.

3.4. Artificial Weathering Test Results

The coatings were exposed to artificial weathering during a 120 h cycle with alternate cycles of rain and UV light, and an inspection was carried out every 24 h.

During the test, the evolution of the samples over time was evaluated with a visual inspection (every 24 h), pictures of which are shown in Figure 10. During the inspections, the WCA was also measured, and it is presented in Figure 11.

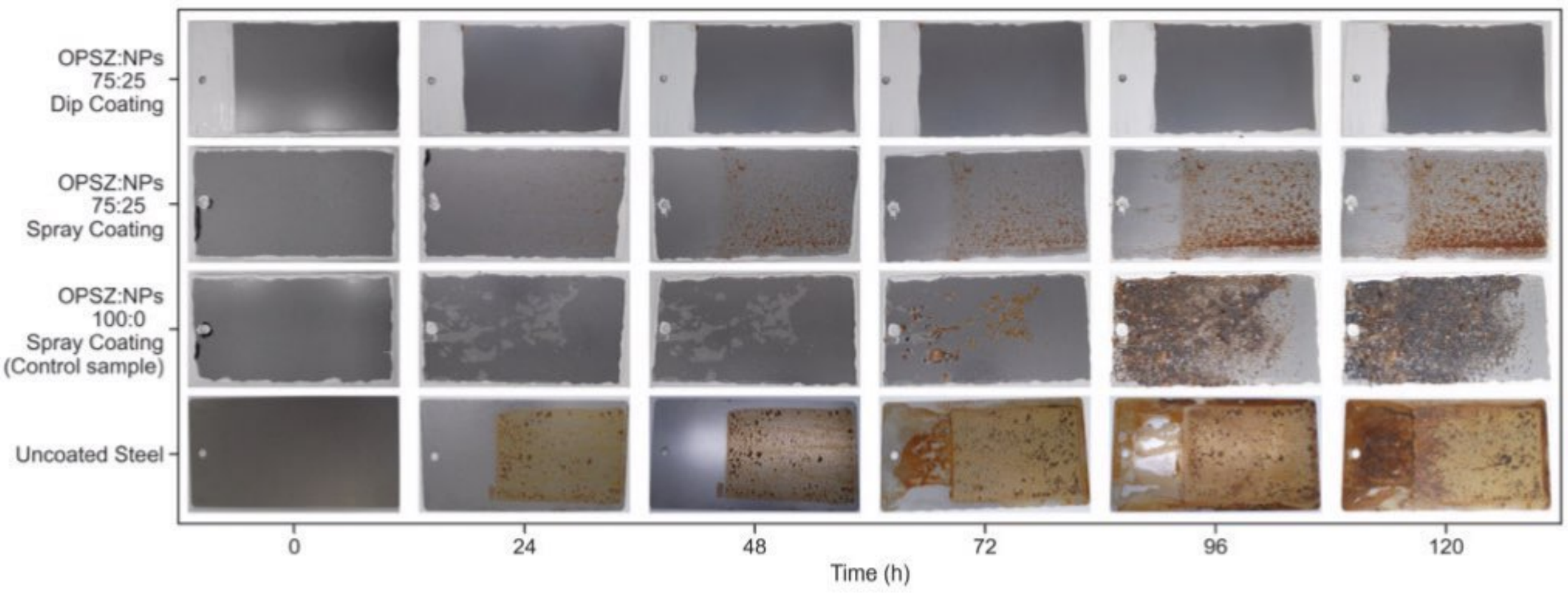

Figure 10. Evolution of coatings on steel during artificial weathering test.

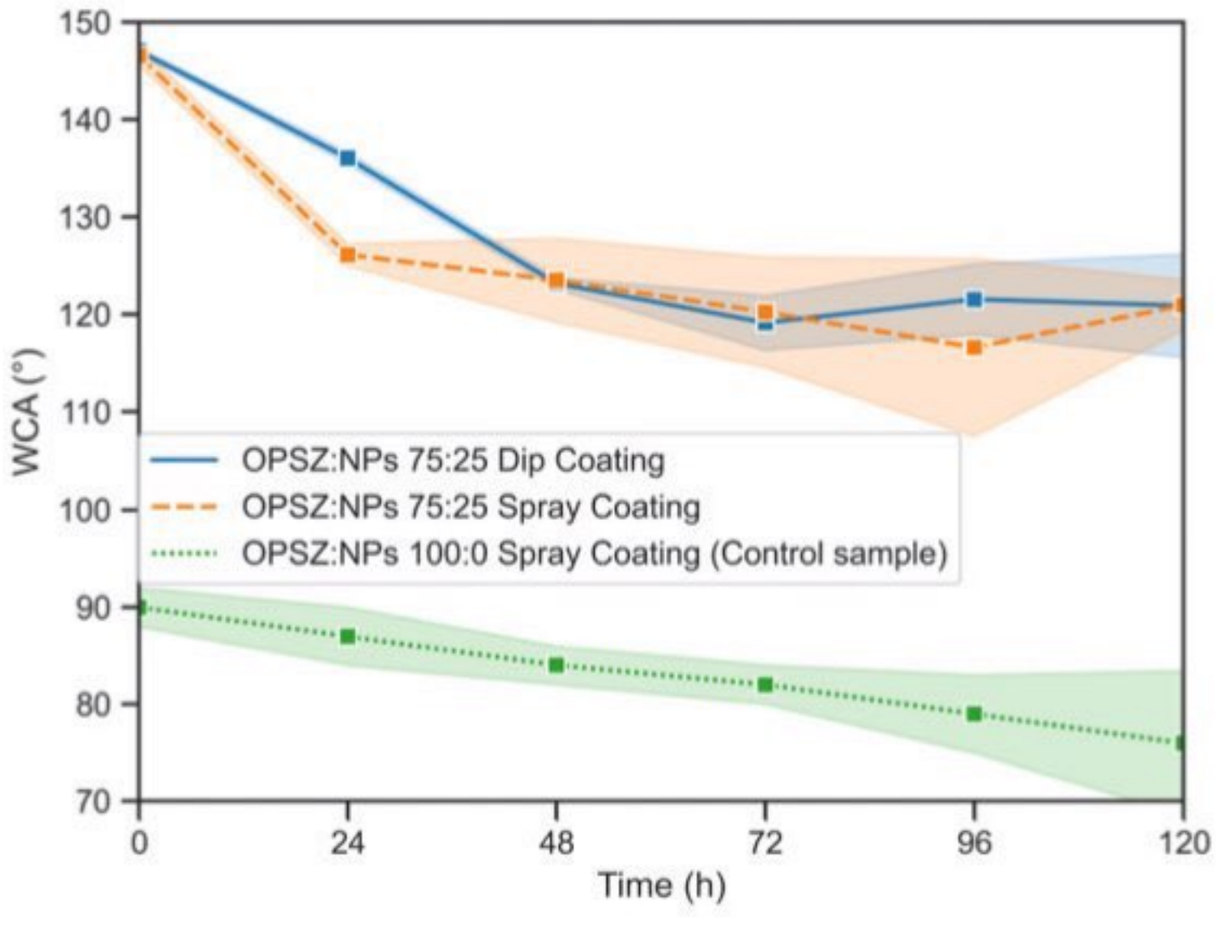

Figure 11. Contact angle measurements versus artificial weathering test time (shadowed area corresponds to the standard deviation).

Before analyzing the results, it should be considered that the artificial weathering test is a severe test, where samples are subjected to thermal shock and UV radiation. In general, both degradation mechanisms promote polymer cracking and color change. In this sense, a clear cracking effect is observed in the control sample (OPSZ:NPs 100:0) following the 24 h exposition. As reported in the literature, numerous cracks appear because of volume shrinkage during the curing process of OPSZs. By adding fillers, this phenomenon is reduced [22].

Otherwise, in the integrated nanoparticle samples, the cracking effect is not detected. This could be explained by the UV light absorption capacity of the SiO_2 nanoparticles and the formation of strong networks between the nanoparticles and polymeric molecules [39].

Regarding the hydrophobic coatings, surface degradation by corrosion is observed in the spray-coated samples (the OPSZ:NPs 75:25 spray coating). Corrosion behavior

similar to that in the salt spray results is observed. The pitting corrosion phenomenon begins to appear early in the control samples and the sprayed coatings with the integrated nanoparticles. However, it is not detected in the dip-coated samples at any time, showing a very good weathering resistance. This corrosion-resistant behavior is very interesting considering the low thickness of the dip-coated samples (5 µm) in comparison to that of the other samples (>29 µm).

Considering the hydrophobic character, it can be observed in Figure 11 that a WCA reduction takes place during the test for both the spray and dip deposition methods, from a highly hydrophobic behavior at t = 0 (~147°) to a hydrophobic behavior (~121°, t = 120 h). This behavior has already been studied by other authors [15].

3.5. EIS Results

The EIS technique was employed to investigate the anticorrosion performance of the coatings. The Bode modulus and Bode phase as well as the Nyquist plots of the coatings analyzed are depicted in Figures 12–14, respectively. Significant differences in the impedance values between the samples were indeed observed.

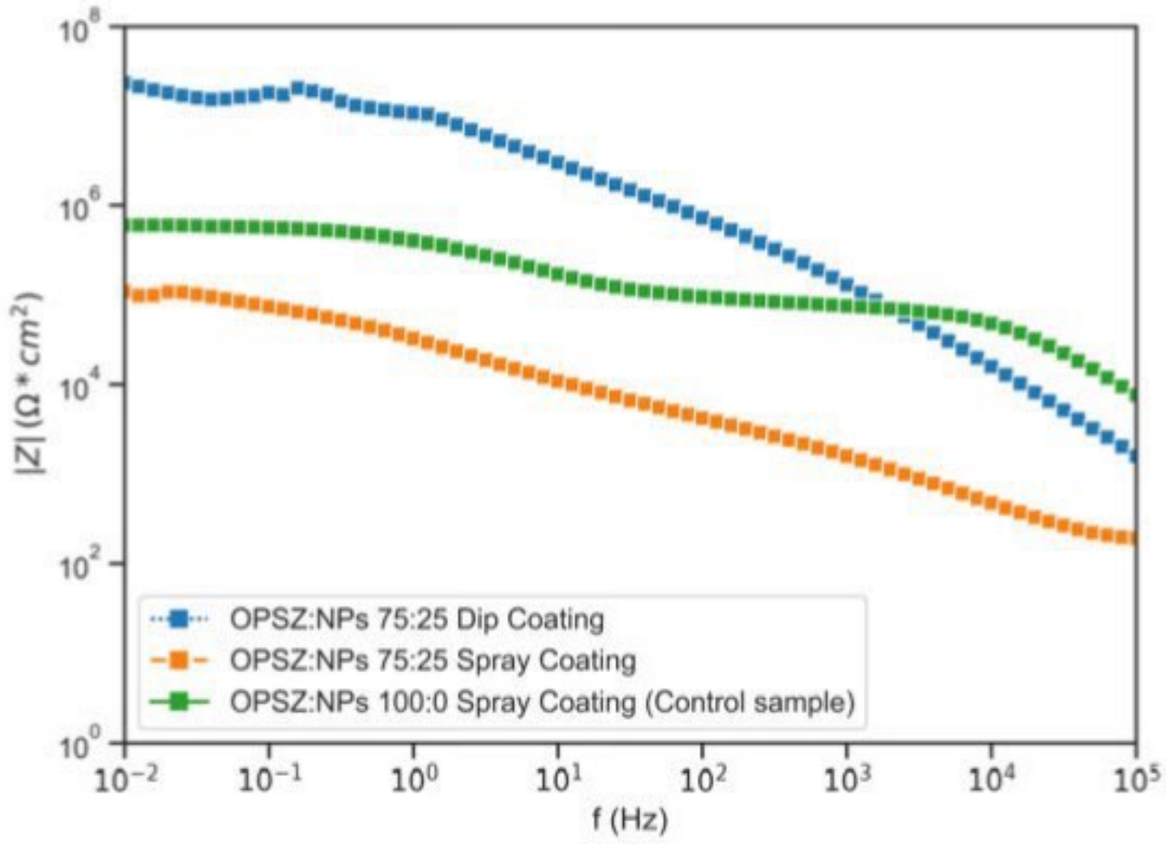

Figure 12. Bode modulus.

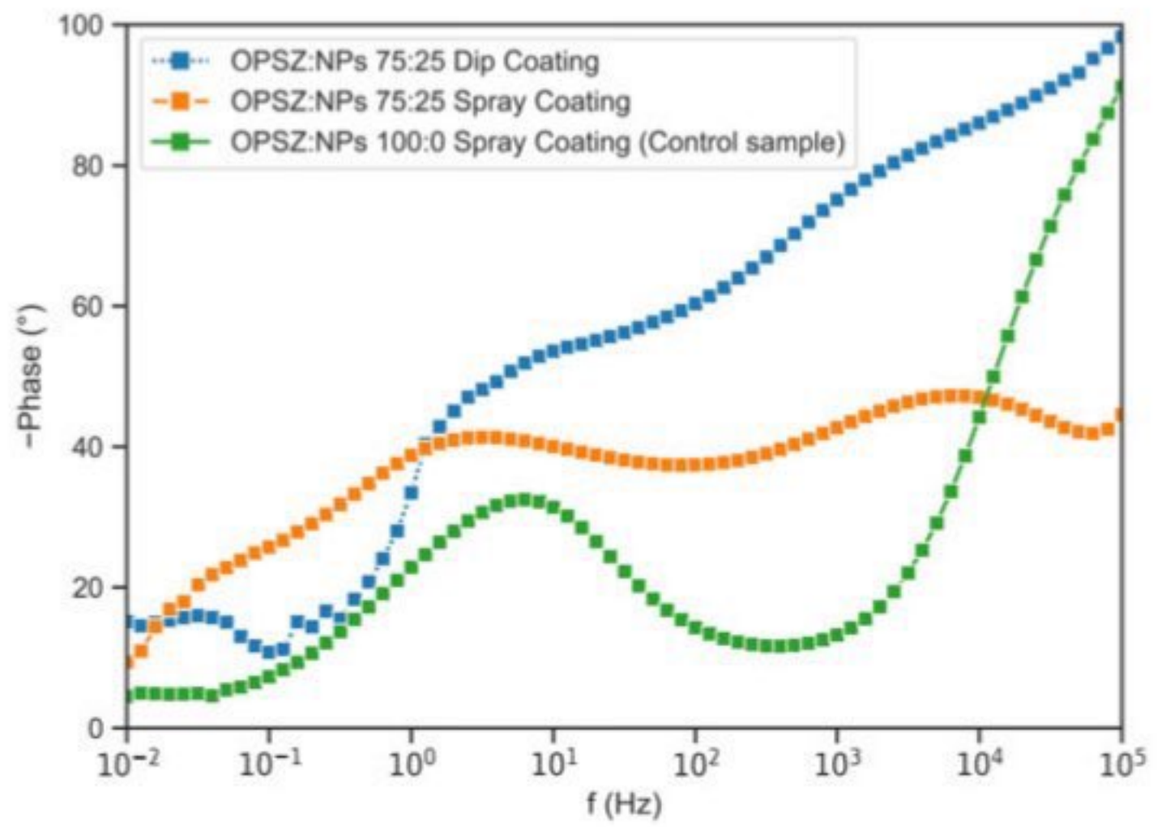

Figure 13. Bode phase.

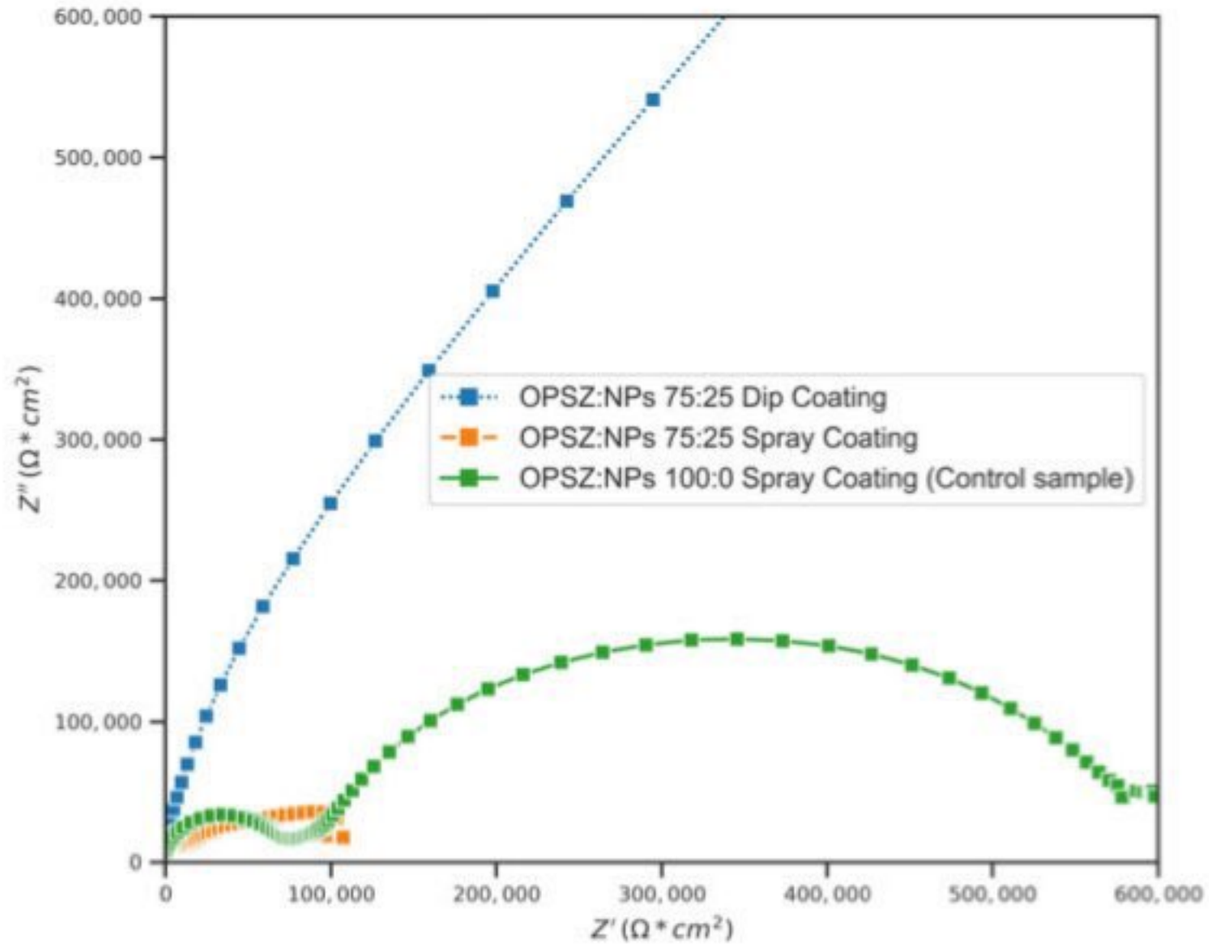

Figure 14. Nyquist plot.

Attending to the Bode modulus plot (Figure 12), the impedance module values, $|Z|$, can be observed at a low frequency, where the highest value corresponds to the dip-coated sample. That is, the dip-coating formulation OPSZ:NPs 75:25 shows the highest impedance modulus in the low-frequency range ($|Z|_{0.0.1\ Hz} = 2.2{\cdot}10^7\ \Omega{\cdot}cm^2$). However, when using the spray-coating technique, the behavior of the system is worse, giving values of the impedance modulus two orders of magnitude lower ($|Z|_{0.0.1\ Hz} = 1.1{\cdot}10^5\ \Omega{\cdot}cm^2$) than those of the dip-coating technique applied to the samples.

The Bode phase plot (Figure 13) properties diminish over time, which means that all the systems are not in the perfect capacitive area whatsoever. This is in accordance with the Nyquist plot (Figure 14), as the coatings treated with the spray-coating technique show an arc far more resistive than that of the dip-coated samples, which is more capacitive and, thus, more likely to reach values of a higher impedance. Additionally, the surfaces of the samples treated using the spray-coating technique show, at high frequencies, a very poor performance on the protective coating side and a very advanced corrosion process at low frequencies due to the existence of pores. This fact allows for the migration of ions from the electrolyte to gain access throughout the net of pores to the metal beneath with considerable ease. The existence of two different arcs depicted by the Nyquist plot explains this electrochemical behavior very well and fits quite well with the visual inspection carried out after the salt spray test (Figure 8).

In addition, considering that the thickness of the dip-coated samples is much smaller than that of the control sample (5 μm vs. 80 μm), the values of impedance clearly confirm the improvement of the barrier effect promoted by the nanoparticle integration into the polymer.

The EIS analyses are consistent with the results obtained from the salt spray and accelerated weathering tests.

4. Conclusions

The hydrophobic performance of OPSZs combined with SIO_2 nanoparticles was investigated. The environmental degradation of the coatings was evaluated by using different tests, namely, salt spray, accelerated weathering and EIS tests, and the main conclusions are as follows:

1. Hydrophobic surfaces were successfully synthesized using a mixture of OPSZs and hydrophobic SiO_2 nanoparticles. At an NP percentage of 25%, the water contact angle

of the coatings was 147° in the horizontal plane, which can be considered highly hydrophobic, very close to the superhydrophobic regime.

2. Two deposition methods (spray-coating and dip-coating methods) were compared. The results clearly depict a higher level of protection when the dip-coating method was used. The spray-coating method is not appropriate for these types of polymers, causing heterogeneities and defects on the surface finish. The dip-coating method is a facile and low-cost method, and a good surface finish is achieved.
3. The hydrophobic effect favors corrosion resistance, but mainly in a marine environment with atmospheric and splash exposures and not in immersion, where the homogeneity of the coating prevails.
4. The formulation OPSZ:NPs 75:25 deposited using the dip-coating method showed a great corrosion resistance in comparison with that of the other samples, assessed by all the degradation tests. This corrosion-resistant behavior is very interesting considering the low thickness of the dip-coated samples (5 μm) in comparison to that of the other samples (>29 μm).

Author Contributions: Conceptualization, L.P.-G., D.A. and A.Y.; methodology, L.P.-G., D.A., C.M., M.G.-B. and L.S.; software, L.S.; validation, L.P.-G., C.M. and M.G.-B.; formal analysis, L.P.-G., D.A. and A.Y.; investigation, L.P.-G., D.A., C.M., M.G.-B. and L.S.; resources, L.P.-G. and A.Y.; data curation, L.P.-G., D.A. and L.S.; visualization, A.C., L.P.-G. and A.Y.; writing—original draft preparation, L.P.-G., A.C. and A.Y.; writing—review and editing, L.P.-G., A.C. and A.Y.; supervision, L.P.-G., A.C. and A.Y.; project administration, L.P.-G. and A.Y.; funding acquisition, L.P.-G. and A.Y. All authors have read and agreed to the published version of the manuscript.

Funding: This research was funded by the Ministry of Science, Innovation and Universities of Spain, through the Torres Quevedo Program, grant number PTQ2018-009743.

Institutional Review Board Statement: Not applicable.

Informed Consent Statement: Not applicable.

Data Availability Statement: Not applicable.

Acknowledgments: We would like to thank Merck KGaA and specially Ralf Grottenmueller, Juergen Mertes and Christoph Landmann for providing organopolysilazane samples and technical assistance. Their support is greatly appreciated. We would also like to thank Alejandro Cabrera Felipe for his support in the technical discussion of the EIS test results.

Conflicts of Interest: The authors declare no conflict of interest. The funders had no role in the design of the study; in the collection, analyses, or interpretation of data; in the writing of the manuscript; or in the decision to publish the results.

References

1. Simpson, J.T.; Hunter, S.R.; Aytug, T. Superhydrophobic Materials and Coatings: A Review. *Rep. Prog. Phys.* **2015**, *78*, 086501. [CrossRef]
2. Mohamed, A.M.A.; Abdullah, A.M.; Younan, N.A. Corrosion Behavior of Superhydrophobic Surfaces: A Review. *Arab. J. Chem.* **2015**, *8*, 749–765. [CrossRef]
3. Cao, L.; Lu, X.; Pu, F.; Yin, X.; Xia, Y.; Huang, W.; Li, Z. Facile Fabrication of Superhydrophobic Bi/Bi2O3 Surfaces with Hierarchical Micro-Nanostructures by Electroless Deposition or Electrodeposition. *Appl. Surf. Sci.* **2014**, *288*, 558–563. [CrossRef]
4. Wu, L.-K.; Hu, J.-M.; Zhang, J.-Q. One Step Sol–Gel Electrochemistry for the Fabrication of Superhydrophobic Surfaces. *J. Mater. Chem. A Mater.* **2013**, *1*, 14471. [CrossRef]
5. Wu, X.; Fu, Q.; Kumar, D.; Ho, J.W.C.; Kanhere, P.; Zhou, H.; Chen, Z. Mechanically Robust Superhydrophobic and Superoleophobic Coatings Derived by Sol–Gel Method. *Mater. Des.* **2016**, *89*, 1302–1309. [CrossRef]
6. Barshilia, H.C.; Ananth, A.; Gupta, N.; Anandan, C. Superhydrophobic Nanostructured Kapton®Surfaces Fabricated through Ar+O2 Plasma Treatment: Effects of Different Environments on Wetting Behaviour. *Appl. Surf. Sci.* **2013**, *268*, 464–471. [CrossRef]
7. Rezaei, S.; Manoucheri, I.; Moradian, R.; Pourabbas, B. One-Step Chemical Vapor Deposition and Modification of Silica Nanoparticles at the Lowest Possible Temperature and Superhydrophobic Surface Fabrication. *Chem. Eng. J.* **2014**, *252*, 11–16. [CrossRef]

8. Blinov, A.V.; Kostyukov, D.A.; Yasnaya, M.A.; Zvada, P.A.; Arefeva, L.P.; Varavka, V.N.; Zvezdilin, R.A.; Kravtsov, A.A.; Maglakelidze, D.G.; Golik, A.B.; et al. Oxide Nanostructured Coating for Power Lines with Anti-Icing Effect. *Coatings* **2022**, *12*, 1346. [CrossRef]
9. Blinov, A.V.; Nagdalian, A.A.; Arefeva, L.P.; Varavka, V.N.; Kudryakov, O.V.; Gvozdenko, A.A.; Golik, A.B.; Blinova, A.A.; Maglakelidze, D.G.; Filippov, D.D.; et al. Nanoscale Composite Protective Preparation for Cars Paint and Varnish Coatings. *Coatings* **2022**, *12*, 1267. [CrossRef]
10. Bai, Y.; Zhang, H.; Shao, Y.; Zhang, H.; Zhu, J. Recent Progresses of Superhydrophobic Coatings in Different Application Fields: An Overview. *Coatings* **2021**, *11*, 116. [CrossRef]
11. Milionis, A.; Loth, E.; Bayer, I.S. Recent Advances in the Mechanical Durability of Superhydrophobic Materials. *Adv. Colloid Interface Sci.* **2016**, *229*, 57–79. [CrossRef]
12. Zhi, J.-H.; Zhang, L.-Z.; Yan, Y.; Zhu, J. Mechanical Durability of Superhydrophobic Surfaces: The Role of Surface Modification Technologies. *Appl. Surf. Sci.* **2017**, *392*, 286–296. [CrossRef]
13. Montemor, M.F. Functional and Smart Coatings for Corrosion Protection: A Review of Recent Advances. *Surf. Coat. Technol.* **2014**, *258*, 17–37. [CrossRef]
14. Carreño, F.; Gude, M.R.; Calvo, S.; Rodríguez de la Fuente, O.; Carmona, N. Synthesis and Characterization of Superhydrophobic Surfaces Prepared from Silica and Alumina Nanoparticles on a Polyurethane Polymer Matrix. *Prog. Org. Coat.* **2019**, *135*, 205–212. [CrossRef]
15. Zhi, D.; Lu, Y.; Sathasivam, S.; Parkin, I.P.; Zhang, X. Large-Scale Fabrication of Translucent and Repairable Superhydrophobic Spray Coatings with Remarkable Mechanical, Chemical Durability and UV Resistance. *J. Mater. Chem. A Mater.* **2017**, *5*, 10622–10631. [CrossRef]
16. Xu, L.; He, J. Fabrication of Highly Transparent Superhydrophobic Coatings from Hollow Silica Nanoparticles. *Langmuir* **2012**, *28*, 7512–7518. [CrossRef] [PubMed]
17. Chen, Z.; Li, G.; Wang, L.; Lin, Y.; Zhou, W. A Strategy for Constructing Superhydrophobic Multilayer Coatings with Self-Cleaning Properties and Mechanical Durability Based on the Anchoring Effect of Organopolysilazane. *Mater. Des.* **2018**, *141*, 37–47. [CrossRef]
18. Kroke, E.; Li, Y.-L.; Konetschny, C.; Lecomte, E.; Fasel, C.; Riedel, R. Silazane Derived Ceramics and Related Materials. *Mater. Sci. Eng. R Rep.* **2000**, *26*, 97–199. [CrossRef]
19. Bhandavat, R.; Feldman, A.; Cromer, C.; Lehman, J.; Singh, G. Very High Laser-Damage Threshold of Polymer-Derived Si(B)CN-Carbon Nanotube Composite Coatings. *ACS Appl. Mater. Interfaces* **2013**, *5*, 2354–2359. [CrossRef]
20. Li, D.; Guo, P.; Guzi de Moraes, E.; Wan, W.; Zou, J.; Colombo, P.; Shen, Z. Structural Study of Disordered SiC Nanowires by Three-Dimensional Rotation Electron Diffraction. *Mater. Res. Express* **2014**, *1*, 045023. [CrossRef]
21. Fedel, M.; Rodríguez Gómez, F.J.; Rossi, S.; Deflorian, F. Characterization of Polyorganosilazane-Derived Hybrid Coatings for the Corrosion Protection of Mild Steel in Chloride Solution. *Coatings* **2019**, *9*, 680. [CrossRef]
22. Wang, G.; Wang, J.; Wang, J.; Chi, Z.; Zhang, G.; Zhou, Z.; Feng, Z.; Xiong, Y. A Sinter Visualization Device for Observing the Relationship Between Fillers and Porosity of Precursor-Derived Ceramic Coatings. *Coatings* **2020**, *10*, 552. [CrossRef]
23. Riedel, R.; Mera, G.; Hauser, R.; Klonczynski, A. Silicon-Based Polymer-Derived Ceramics: Synthesis Properties and Applications-A Review. *J. Ceram. Soc. Jpn.* **2006**, *114*, 425–444. [CrossRef]
24. Hu, L.; Zhang, L.; Wang, D.; Lin, X.; Chen, Y. Fabrication of Biomimetic Superhydrophobic Surface Based on Nanosecond Laser-Treated Titanium Alloy Surface and Organic Polysilazane Composite Coating. *Colloids Surf. A Physicochem. Eng. Asp.* **2018**, *555*, 515–524. [CrossRef]
25. Huang, X.; Wang, D.; Hu, L.; Song, J.; Chen, Y. Preparation of a Novel Antibacterial Coating Precursor and Its Antibacterial Mechanism. *Appl. Surf. Sci.* **2019**, *465*, 478–485. [CrossRef]
26. Rossi, S.; Deflorian, F.; Fedel, M. Polysilazane-Based Coatings: Corrosion Protection and Anti-Graffiti Properties. *Surf. Eng.* **2019**, *35*, 343–350. [CrossRef]
27. Coan, T.; Barroso, G.S.; Machado, R.A.F.; de Souza, F.S.; Spinelli, A.; Motz, G. A Novel Organic-Inorganic PMMA/Polysilazane Hybrid Polymer for Corrosion Protection. *Prog. Org. Coat.* **2015**, *89*, 220–230. [CrossRef]
28. Available online: https://www.geogebra.org/classic (accessed on 23 December 2021).
29. Montemor, M.F. *Smart Composite Coatings and Membranes*; Elsevier: Amsterdam, The Netherlands, 2016; ISBN 9781782422839.
30. *ISO 16773-4:2017*; Electrochemical Impedance Spectroscopy (EIS) on Coated and Uncoated Metallic Specimens—Part 4: Examples of Spectra of Polymer-Coated and Uncoated Specimens. International Organization for Standardization: Geneva, Switzerland, 2017.
31. Dickie, R.A.; Floyd, F.L. Polymeric Materials for Corrosion Control: An Overview. In *Polymeric Materials for Corrosion Control*; American Chemical Society: Washington, WA, USA, 1986; pp. 1–16.
32. Cai, C.; Sang, N.; Teng, S.; Shen, Z.; Guo, J.; Zhao, X.; Guo, Z. Superhydrophobic Surface Fabricated by Spraying Hydrophobic R974 Nanoparticles and the Drag Reduction in Water. *Surf. Coat. Technol.* **2016**, *307*, 366–373. [CrossRef]
33. Karmouch, R.; Ross, G.G. Superhydrophobic Wind Turbine Blade Surfaces Obtained by a Simple Deposition of Silica Nanoparticles Embedded in Epoxy. *Appl. Surf. Sci.* **2010**, *257*, 665–669. [CrossRef]
34. Manoudis, P.N.; Karapanagiotis, I.; Tsakalof, A.; Zuburtikudis, I.; Panayiotou, C. Superhydrophobic Composite Films Produced on Various Substrates. *Langmuir* **2008**, *24*, 11225–11232. [CrossRef]

35. Chatzigrigoriou, A.; Karapanagiotis, I.; Poulios, I. Superhydrophobic Coatings Based on Siloxane Resin and Calcium Hydroxide Nanoparticles for Marble Protection. *Coatings* **2020**, *10*, 334. [CrossRef]
36. Chavez, R.; Ionescu, E.; Balan, C.; Fasel, C.; Riedel, R. Effect of Ambient Atmosphere on Crosslinking of Polysilazanes. *J. Appl. Polym. Sci.* **2011**, *119*, 794–802. [CrossRef]
37. Barkhudarov, P.M.; Shah, P.B.; Watkins, E.B.; Doshi, D.A.; Brinker, C.J.; Majewski, J. Corrosion Inhibition Using Superhydrophobic Films. *Corros. Sci.* **2008**, *50*, 897–902. [CrossRef]
38. Ou, J.; Liu, M.; Li, W.; Wang, F.; Xue, M.; Li, C. Corrosion Behavior of Superhydrophobic Surfaces of Ti Alloys in NaCl Solutions. *Appl. Surf. Sci.* **2012**, *258*, 4724–4728. [CrossRef]
39. Yedra, A.; Gutiérrez-Somavilla, G.; Manteca-Martínez, C.; González-Barriuso, M.; Soriano, L. Conductive Paints Development through Nanotechnology. *Prog. Org. Coat.* **2016**, *95*, 85–90. [CrossRef]